



## RESEARCH ARTICLE

10.1029/2018JD029802

## Key Points:

- Two years of in situ measurements of the number concentrations of Arctic cloud particles ( $N_c$ ) show a clear seasonal variation with a maximum in summer
- Aerosols with diameters as small as 30 nm likely serve as cloud condensation nuclei (CCN) due to the low CCN concentrations in the Arctic
- The aerosol-cloud interaction (ACI) index for CCN-controlled clouds was estimated to be approximately 0.22, and it does not show a clear seasonal variation

## Correspondence to:

M. Koike,  
koike@eps.s.u-tokyo.ac.jp

## Citation:

Koike, M., Ukita, J., Ström, J., Tunved, P., Shiobara, M., Vitale, V., et al. (2019). Year-round in situ measurements of Arctic low-level clouds: Microphysical properties and their relationships with aerosols. *Journal of Geophysical Research: Atmospheres*, 124, 1798–1822. <https://doi.org/10.1029/2018JD029802>

Received 11 OCT 2018

Accepted 19 JAN 2019

Accepted article online 25 JAN 2019

Published online 15 FEB 2019

## Author Contributions:

**Conceptualization:** M. Koike**Data curation:** J. Ström, P. Tunved, M. Shiobara, V. Vitale, A. Lupi, D. Baumgardner, C. Ritter, O. Hermansen, K. Yamada, C. A. Pedersen**Funding acquisition:** J. Ukita, O. Hermansen**Investigation:** M. Koike, J. Ukita, J. Ström, P. Tunved, D. Baumgardner, C. Ritter**Methodology:** M. Koike  
(continued)**Methodology:** M. Koike

(continued)

## Year-Round In Situ Measurements of Arctic Low-Level Clouds: Microphysical Properties and Their Relationships With Aerosols

M. Koike<sup>1</sup> , J. Ukita<sup>2</sup>, J. Ström<sup>3</sup>, P. Tunved<sup>3</sup>, M. Shiobara<sup>4</sup>, V. Vitale<sup>5</sup>, A. Lupi<sup>5</sup>, D. Baumgardner<sup>6</sup>, C. Ritter<sup>7</sup>, O. Hermansen<sup>8</sup>, K. Yamada<sup>4</sup> , and C. A. Pedersen<sup>9</sup>

<sup>1</sup>Department of Earth and Planetary Science, Graduate School of Science, University of Tokyo, Tokyo, Japan, <sup>2</sup>Faculty of Science, Niigata University, Niigata, Japan, <sup>3</sup>Department of Environmental Science and Analytical Chemistry, Stockholm University, Stockholm, Sweden, <sup>4</sup>National Institute of Polar Research, Tokyo, Japan, <sup>5</sup>Institute of Atmospheric Sciences and Climate (ISAC)/Italian National Research Council (CNR), Bologna, Italy, <sup>6</sup>Droplet Measurement Technologies, Longmont, CO, USA, <sup>7</sup>Alfred Wegener Institute, Potsdam, Germany, <sup>8</sup>Norwegian Institute for Air Research (NILU), Oslo, Norway, <sup>9</sup>Norwegian Polar Institute, Tromsø, Norway

**Abstract** Two years of continuous in situ measurements of Arctic low-level clouds have been made at the Mount Zeppelin Observatory (78°56'N, 11°53'E), in Ny-Ålesund, Spitsbergen. The monthly median value of the cloud particle number concentration ( $N_c$ ) showed a clear seasonal variation: Its maximum appeared in May–July ( $65 \pm 8 \text{ cm}^{-3}$ ), and it remained low between October and March ( $8 \pm 7 \text{ cm}^{-3}$ ). At temperatures warmer than 0 °C, a clear correlation was found between the hourly  $N_c$  values and the number concentrations of aerosols with dry diameters larger than 70 nm ( $N_{70}$ ), which are proxies for cloud condensation nuclei (CCN). When clouds were detected at temperatures colder than 0 °C, some of the data followed the summertime  $N_c$  to  $N_{70}$  relationship, while other data showed systematically lower  $N_c$  values. The lidar-derived depolarization ratios suggested that the former (CCN-controlled) and latter (CCN-uncontrolled) data generally corresponded to clouds consisting of supercooled water droplets and those containing ice particles, respectively. The CCN-controlled data persistently appeared throughout the year at Zeppelin. The aerosol-cloud interaction index ( $\text{ACI} = \text{dln}N_c / (3\text{dln}N_{70})$ ) for the CCN-controlled data showed high sensitivities to aerosols both in the summer (clean air) and winter–spring (Arctic haze) seasons ( $0.22 \pm 0.03$  and  $0.25 \pm 0.02$ , respectively). The air parcel model calculations generally reproduced these values. The threshold diameters of aerosol activation ( $D_{\text{act}}$ ), which account for the  $N_c$  of the CCN-controlled data, were as low as 30–50 nm when  $N_{70}$  was less than  $30 \text{ cm}^{-3}$ , suggesting that new particle formation can affect Arctic cloud microphysics.

### 1. Introduction

The annual average Arctic temperature has increased at almost twice the rate as that of the rest of the world over the past few decades (IPCC, 2013). The main driver of this warming is an increase in the global concentration of carbon dioxide; however, various other climate forcings and feedback processes are amplifying the magnitude of warming in the Arctic (e.g., Serreze & Barry, 2011). In the Arctic, cloud radiative forcing at the surface is positive throughout the year, except during a short time period in summer (Curry & Ebert, 1992), and it is considered to play a significant role in the recent warming in the Arctic (e.g., Graversen & Wang, 2009). In fact, possible changes in the cloud amounts in the Arctic associated with changes in the sea ice have been reported (e.g., Palm et al., 2010).

Aerosols, which can act as cloud condensation nuclei (CCN) and ice-nucleating particles (INP), can affect Arctic clouds (i.e., indirect effects). In addition to the shortwave cloud albedo effect that is exerted all over the globe (Twomey, 1977), the cloud particle size dependence of longwave emissivity can result in a positive radiative forcing at the Arctic surface, partly because the optical thickness of Arctic clouds is generally thin (Garrett & Zhao, 2006; Lubin & Vogelmann, 2006). In the Arctic, very low CCN concentrations ( $<10 \text{ cm}^{-3}$ ) also affect precipitation, such that a small increase in aerosol concentrations may enhance cloudiness (Mauritsen et al., 2011). Furthermore, CCN and INP can affect mixed-phase clouds by exerting impacts on glaciation, riming, and secondary ice production processes (e.g., Jackson et al., 2012; Lohmann & Feichter, 2005).

©2019. The Authors.

This is an open access article under the terms of the Creative Commons Attribution-NonCommercial-NoDerivs License, which permits use and distribution in any medium, provided the original work is properly cited, the use is non-commercial and no modifications or adaptations are made.

**Supervision:** J. Ukita, D. Baumgardner, O. Hermansen  
**Writing - original draft:** M. Koike  
**Writing - review & editing:** J. Ukita, J. Ström, P. Tunved, V. Vitale, D. Baumgardner, C. Ritter, O. Hermansen

In general, the existence of aerosol-induced impacts on cloud microphysics is not in question. However, quantification of the impacts has large uncertainties. As a measure of the sensitivity of aerosol impacts on cloud microphysics, the aerosol-cloud interaction (ACI) index, defined below, has been widely used (e.g., McComiskey & Feingold, 2012):

$$ACI = \frac{1}{3} \frac{d \ln N_c}{d \ln N_a} \text{ or } - \left. \frac{\partial \ln r_e}{\partial \ln N_a} \right|_{CWC} \quad (1)$$

where  $N_c$ ,  $N_a$ ,  $r_e$ , and CWC are the cloud particle number concentration, aerosol number concentration, cloud effective radius, and cloud water content, respectively. The two expressions of the ACI index in equation (1) become equal when  $r_e \propto N_c^{-1/3}$  at a constant CWC. The ACI index can take values between 0 and 0.33. In previous studies, these types of indices (or the slopes of the relationships between aerosols and clouds) have been used to evaluate the ability of general circulation models to represent aerosol-cloud interactions by comparing the index values (or slopes) between observations and numerical model calculations. Several assessment studies of general circulation model calculations using satellite measurements have been reported (e.g., Quaas et al., 2009), although the relatively large areal scales of satellite data analyses tend to introduce errors in the estimates (McComiskey & Feingold, 2012). Because in situ measurements of clouds are limited in the Arctic, the ACI index values have been estimated using ground-based or satellite remote sensing. In these studies, tracer transport models or global chemistry models have also been used to estimate aerosol amounts. As a result, ACI index values between 0.0 and 0.19 were derived (Coopman et al., 2016; Garrett et al., 2004; Tietze et al., 2011), although values close to 0.33 were derived in limited cases (Coopman et al., 2018). By combining the in situ measurements made during several aircraft experiments in the Arctic, ACI index values of approximately 0.16 were also derived (Zamora et al., 2016). More reliable estimates of the ACI index in the Arctic/northern high latitudes were made using multiyear data from ground-based in situ measurements in the Pallas area of northern Finland (68°N, 24°E), and ACI index values between 0.2 and 0.3 were obtained (Lihavainen et al., 2010). However, the number of reliable estimates available to evaluate aerosol-cloud interactions remains quite limited in the Arctic.

In situ measurements of Arctic clouds and aerosols were made during various aircraft experiments over the past 10 years (e.g., Brock et al., 2011; Jourdan et al., 2010; Klingebiel et al., 2015; McFarquhar et al., 2011; Verlinde et al., 2007; Young et al., 2016). In situ measurements of clouds/fogs in the Arctic or northern high latitudes were also made from the ground (e.g., Gultepe et al., 2014; Lihavainen et al., 2010; Uchiyama et al., 2014). Although these measurements revealed various important aspects of Arctic clouds and their relationships with aerosols, the measurements were only made during limited time periods; therefore, conclusions were generally derived from specific case studies. Year-round in situ measurements of the microphysical properties of clouds have not previously been made, and therefore, the year-round relationships between clouds and aerosols have also not been studied.

Regarding the aerosol measurements, continuous and long-term in situ measurements have been made in Ny-Ålesund (Engvall et al., 2008; Strom et al., 2003; Tunved et al., 2013), and a clear seasonal variation has been identified. The period between March and May is characterized by dominantly accumulation-mode aerosols due to the buildup of anthropogenic aerosols over the Arctic, which is known as Arctic haze. The period between June and August is characterized by low and high concentrations of accumulation- and Aitken-mode aerosols, respectively. The dominance of Aitken-mode aerosols is likely caused by frequent new particle formation (Tunved et al., 2013), although primary sea spray aerosols could also contribute to the formation of this aerosol mode (e.g., Quinn et al., 2015). A sharp transition in the aerosol size distribution was observed from April to June, during which the fraction of the Aitken-mode aerosols increased. The period between September and February is characterized by comparably low concentrations of accumulation- and Aitken-mode aerosols, although accumulation-mode aerosols gradually increase toward the spring maximum, likely due to the buildup of anthropogenic aerosols.

To characterize the microphysical properties of Arctic low-level clouds and their year-round variations, in situ measurements of cloud particles began at the Mount Zeppelin Observatory (78°56'N, 11°53'E, 474 m above mean sea level (asl)) in Ny-Ålesund, Spitsbergen, in October 2013. In June 2014, size distribution measurements of the precipitating particles using an optical disdrometer also began. In this paper, we report the seasonal variations in the microphysical properties of clouds and their relationships to

**Table 1**  
*List of Instruments*

Instrument	Measured parameters	Sampling frequency	Accuracy	Location	References
FM-120 (fog monitor)	Number size distributions of cloud particles with radii between 1.5 and 23.5 $\mu\text{m}$	10 s	$\pm 20\%$ (cloud particle number concentrations, $N_c$ )	Zeppelin Observatory	Spiegel et al. (2012) <sup>a</sup> ; Guyot et al. (2015) <sup>a</sup>
MPS (optical disdrometer)	Number size distributions of the precipitating particles with radii between 12.5 and 775 $\mu\text{m}$	10 s	$\pm 70\%$ (precipitating particle number concentrations)	Zeppelin Observatory	Bringi et al. (2018) <sup>a</sup>
DMPS	Number size distributions of aerosols with dry diameters between 5 and 809 nm	20 min	$\pm 20\%$	Zeppelin Observatory	Engvall et al. (2008); Strom et al. (2003); Tunved et al. (2013)
TSI SMPS 3034 (scanning mobility particle sizer)	Number size distributions of aerosols with dry diameters between 10 and 470 nm	10 min	$\pm 10\%$	Gruvebadet Observatory	Lupi et al. (2016)
Meteorological instruments (Vaisala)	Temperature, horizontal wind speed/direction (vane and three-cup anemometer)	60 min	$\pm 0.2$ K for temperature, $\pm 0.3$ m/s for wind speed	Zeppelin Observatory at an altitude of 15 m above the ground surface	
Ultrasonic anemometer (Metek uSonic-3)	3-D wind speed/direction	1 s	$\pm 0.1$ m/s or 2%	Zeppelin Observatory at an altitude of 2.3 m above the ground surface	
Cielometer (Vaisala, CL 51)	Cloud base height	60 min	$\pm 1\%$ or 5 m	AWI station	Maturilli and Ebell (2018)
Micropulse lidar (Sigma Space, MPL-4B-IDS-532)	Depolarization ratio of particles at wavelength of 532 nm	1 min	Not available	AWI station and Rabben Observatory before and after March 2015, respectively	

*Note.* Zeppelin Observatory and Gruvebadet Observatory are located near the mountaintop and the mountain base, respectively. Locations of the observatories are shown in Figure 1b. For the DMPS measurements, the whole air inlet was used to measure both interstitial aerosols and aerosols within cloud particles, by evaporating them within the heated inlet tube. MPS = Meteorological Particle Sensor; DMPS = differential mobility particle sizer; AWI = Alfred Wegener Institute.

<sup>a</sup>Studies made at locations other than Ny-Ålesund.

aerosols by focusing on the ACI index values in summer (clean air) and winter–spring (Arctic haze) as the definitive metric.

## 2. Measurements

The instruments used in this study are listed in Table 1, and the locations of the observatories are illustrated in Figure 1.

### 2.1. Local Meteorological Conditions

Figure 2 shows the daily average atmospheric temperatures observed at Zeppelin for both cloudy days and days with no clouds. Here we define cloudy days as those when “in-cloud” data (cloud water content,  $\text{CWC} > 0.01 \text{ g/m}^3$ , section 2.2.) were obtained for more than 10 min at the Mount Zeppelin Observatory. The presence of clouds was locally judged at Zeppelin; clouds could still exist at higher altitudes on “no-clouds” days. Temperatures  $> 0^\circ\text{C}$  are generally limited to July and August, when clouds are expected to consist of water droplets. During the rest of the year, supercooled water droplets and/or ice particles are expected to be observed at Zeppelin.

Figure 3 shows the statistics of the horizontal wind direction/speed at Zeppelin measured with a Vaisala instrument (15 m above the ground surface, section 2.5) when in-cloud data were obtained. All available data between 2013 and 2015 were used for the results shown here for January, April, July, and October. Although the time duration of the data used for this statistical analysis is limited due to the relatively low

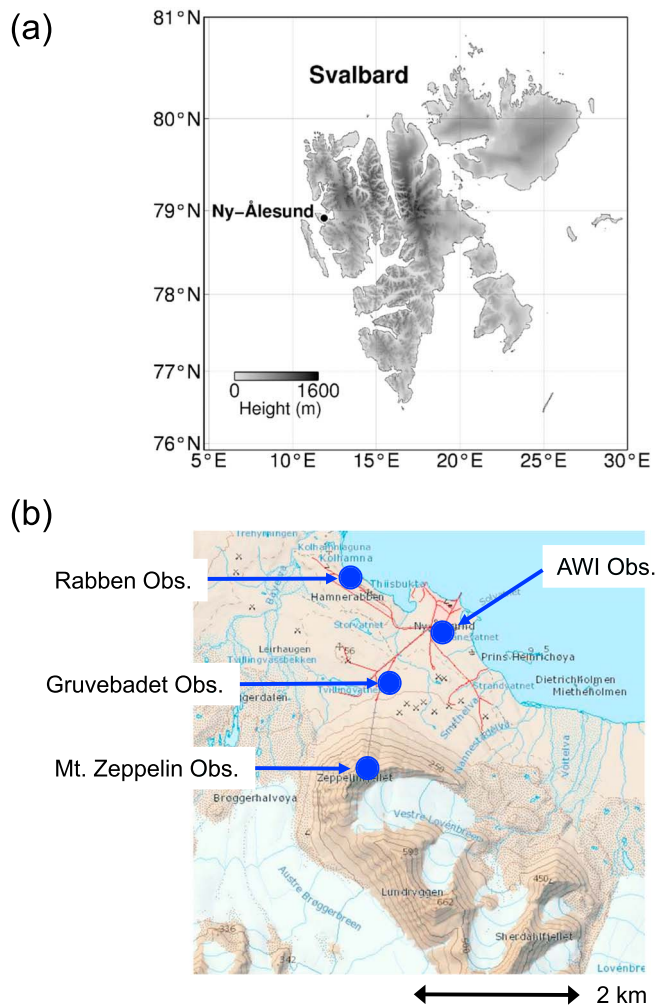


**Figure 1.** (a) Map of Svalbard showing the location of Ny-Ålesund. (b) Map showing the locations of the observatories in Ny-Ålesund. A list of the instruments at these observatories is given in Table 1. This map was obtained from the Norwegian Polar Institute web site (<http://www.npolar.no/en/services/maps/>).

frequency of cloud detection, especially in the winter (section 3.1), the features shown in this figure are generally similar to those obtained by the statistical analysis of all of the wind data (irrespective of the presence of clouds). Southerly or southeasterly winds were frequently observed throughout the entire year, and northwesterly winds were also observed in the spring and fall. The inlet of the fog monitor (FM-120) was oriented toward the south to minimize particle losses (section 2.2). Some particle loss is expected, especially for large cloud droplets in the spring under northwesterly, high-speed wind conditions. These uncertainties are described later (section 2.2 and Appendix B).

Previous studies have suggested that the wind field and thermal structure of the lowest altitudes around Ny-Ålesund are strongly influenced by the katabatic flow from the Kongsvegen glacier, which is located to the east of Ny-Ålesund (Beine et al., 2001; Esau & Repina, 2012). The local wind direction at the Mount Zeppelin Observatory is additionally affected by the surrounding orography, and it generally originates from a southerly direction (Beine et al., 2001). Notably, horizontal wind speeds measured near the FM-120 (2.3 m above the ground surface) were systematically slower than those measured at an altitude of 15 m (Vaisala instrument), suggesting that very local horizontal wind around the instruments is likely further influenced by the friction of the ground surface (Appendix A).

It is beyond the scope of this work to describe the meteorological conditions that lead to cloud formation at Mount Zeppelin; however, we note that, in general, clouds with cloud base heights lower than 500 m were detected by the ceilometer at the Alfred Wegener Institute (AWI) site (section 2.5) when clouds were detected by the FM-120 at Mount Zeppelin (474 m asl). Because these two measurements were made 2.1 km apart in horizontal distance, this result suggests that the low-level clouds detected at Zeppelin were not very local clouds limited only to the area around the mountaintop. Moreover, cloud images obtained by the satellite-borne MODerate resolution Imaging Spectroradiometer instrument show that clouds were generally spread over a distance of more than 1,000 km (over the Greenland and Barents Seas) when clouds were detected at Zeppelin. Consequently, the results presented in this study are considered to represent the microphysical properties of part of these widespread clouds, although the properties can be quite different due to the local meteorology and aerosol sources.

## 2.2. Fog Monitor (FM-120)

In situ measurements of the cloud particle size distributions with radii between 1.5 and 23.5  $\mu\text{m}$  were continuously made using a fog monitor (FM-120, DMT Inc., CO USA), which has been located on the deck of the Zeppelin Observatory since October 2013. This instrument records the pulse heights of the light scattered by individual particles that pass through a focused 685-nm laser beam. The particle radii are derived from these signals using Mie scattering theory and by assuming that these particles are spherical water droplets (Spiegel et al., 2012). An aspiration fan is attached to the downstream side of the probe, and it draws the air through the sample area at an air speed of approximately 12 m/s, which is monitored using a Pitot tube. The in-focus area of the detector is 0.24  $\text{mm}^2$ ; thus, the sensing volume of air within a 10-s integration time is 29  $\text{cm}^3$ . Calibrations of the particle size measurements were performed once or twice a year by introducing glass beads into the probe (Duke Scientific Inc.), and no apparent changes were detected. Measurement uncertainties are discussed in greater detail in Appendix B.

The cloud particle number concentration,  $N_c$ , reported in this paper represents particles with radii between 1.5 and 23.5  $\mu\text{m}$ . The CWC values were obtained by integrating the size distribution of the cloud particles

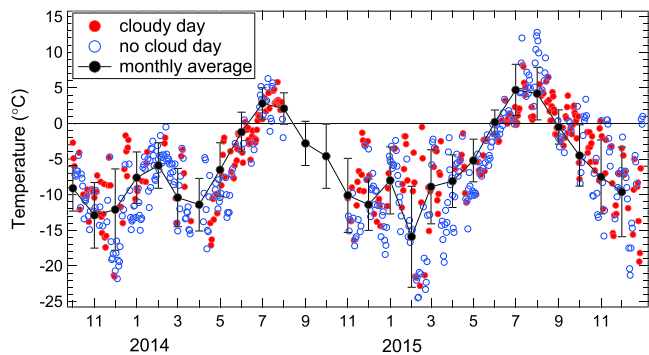


**Figure 2.** Daily and monthly mean temperatures at the Mount Zeppelin Observatory. The black closed circles and vertical bars represent the monthly means and standard deviations, respectively, for which data from both cloudy days and no cloud days are used. The daily mean temperature values for cloudy days and days with no clouds are shown separately. See the text for the definition of cloudy days (cloud measurements were not made between August and October 2014, and therefore, no information on the presence of clouds was available).

( $r = 1.5\text{--}23.5 \mu\text{m}$ ), assuming that the particles are spherical. We define data as in-cloud when the 10-s average CWC value was greater than  $0.01 \text{ g/m}^3$ . This threshold value for CWC is the same as that used in our previous aircraft studies (Koike et al., 2012), and the 10-s integration time was chosen to increase the air sample volume to reduce counting fluctuations. In this study, we used 1-hr averages, which are calculated only using in-cloud data.

Various artifacts can be expected when using an aspiration system. Both the theoretical and numerical analyses for FM-100 (which is basically the same as FM-120) suggest that particle losses during sampling are typically less than 10% for a droplet radius ( $r$ ) of up to  $5 \mu\text{m}$ ; however, they can be greater than 90% for  $r = 25 \mu\text{m}$  when the angle between the inlet orientation and the wind vector (i.e., the sampling angle,  $\theta$ ) becomes large (Spiegel et al., 2012). Guyot et al. (2015) suggested from FM-100 measurements that particle losses decrease with increasing wind speed for  $\theta < 30^\circ$ , while they increase with increasing wind speed for  $\theta > 30^\circ$ , especially for large particles. In this study, the inlet of the FM-120 was oriented toward the south, which is the prevailing wind direction at Zeppelin (section 2.1), to minimize particle losses. However, we occasionally sampled cloud particles

with sampling angles greater than  $30^\circ$ , especially in the spring and fall as well as under various wind speed conditions (section 2.1); under these conditions, anisokinetic sampling of large particles may have occurred.

As discussed in Appendix A, we examined the possible errors in  $N_c$  and CWC by comparing their values obtained under various sampling angles and wind speeds. As a result, no clear signature of particle losses was found for  $N_c$ . The CWC values decreased with increasing wind speed when  $\theta > 30^\circ$ , and this tendency could be partly due to particle losses because CWC is more sensitive to losses of large particles. However, these CWC values were not necessarily lower than the values obtained with  $\theta < 30^\circ$ , which are considered to be more reliable. Based on these results, we have not made any corrections of the data and have not rejected any data in this study.

In Appendix B, we also show that the monthly median values of  $N_c$  and CWC obtained in this study are generally similar to those calculated using only data with  $\theta < 30^\circ$ , which are considered to be less affected by

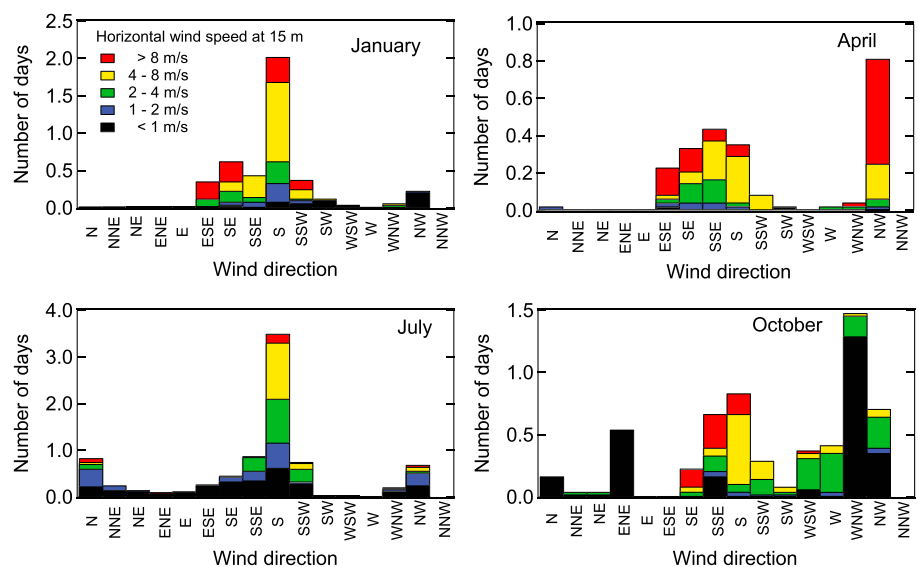


**Figure 3.** Statistics of horizontal wind direction and speed at the Mount Zeppelin Observatory (hourly data) when the “in-cloud” data were obtained. Wind data measured at an altitude of 15 m by the Vaisala instrument ( $U_{15}$ , Table 1) were used as meteorological data. Notably, horizontal wind speeds measured near the fog monitor (2.3 m above the ground surface) were systematically slower than those measured at an altitude of 15 m (Appendix A).

particle losses. The median values for the monthly  $N_c/N_{c_{\theta < 30}}$  ratios and  $CWC/CWC_{\theta < 30}$  ratios were 1.05 (with a 25–75% range of 0.77–1.50) and 1.00 (with a 25–75% range of 0.91–1.06), respectively. The relatively small changes in the  $N_c$  and CWC values were because the number fractions of the large particles are generally small. In summary, the influences of particle losses on the cloud microphysical properties shown in this paper are estimated to be generally small.

### 2.3. Optical Disdrometer

In situ measurements of the precipitating particle size distributions with radii between 12.5 and 775  $\mu\text{m}$  (12.5  $\mu\text{m}$  resolution) were continuously made using an optical disdrometer, a Meteorological Particle Sensor (MPS, DMT Inc., Bringi et al., 2018), since June 2014. The MPS measures the size, shape, and fall velocity of individual precipitating particles using the technique first introduced by Knollenberg (1970, 1981). In short, the MPS is an optical array probe with a 64-element photodiode array that is illuminated with a 660-nm collimated laser beam. Droplets cast a shadow on the array as they gravitationally fall through the laser. The subsequent decrease in light intensity on the diodes is detected, and a two-dimensional image is captured by recording the light level of each diode during the period in which the array is shadowed. The fall velocity is derived from the maximum horizontal dimension (spherical drop shape assumption) divided by the amount of time that the image is on the array (measured with a 2-MHz clock). A wind vane on the MPS maintains the diode array perpendicular to the average wind direction to minimize uncertainties related to the direction of the horizontal wind. Because of the relatively large uncertainties in the estimates of the precipitation rates derived from the MPS-measured size distribution and fall speeds, this information is used only for broad classifications in this study: We classify data into three precipitation rate categories, namely, less than 0.01, between 0.01 and 1, and greater than 1 mm/day.

### 2.4. Measurements of the Aerosol Size Distribution

The number size distributions of aerosols with dry diameters between 5 and 809 nm were measured at the Mount Zeppelin Observatory using a differential mobility particle sizer (DMPS, Table 1; Engvall et al., 2008; Strom et al., 2003; Tunved et al., 2013). Each scan over the particle size range takes 20 min; we used 1-hr averages in this study. A whole air inlet was used for these measurements. This inlet was originally designed for the Jungfraujoch station in Switzerland to measure aerosols on a mountaintop, including those within cloud/fog particles, by evaporating them within the heated inlet tube (Weingartner et al., 1999). The use of this inlet has been recommended by the World Calibration Center for Aerosol Physics (<http://www.wmo-gaw-wcc-aerosol-physics.org/>) when all aerosols are to be measured. The whole air inlet at Zeppelin is approximately 2.5 m above the roof, and the sample air flow rate is 100 L/min. Some of the sample air was analyzed using the DMPS. Possible errors due to the use of the whole air inlet are described in Appendix C.

The number size distributions of aerosols with dry diameters between 10 and 470 nm were also measured at the Gruvebadet Observatory at the base of Mount Zeppelin (67 m asl, Figure 1b) using a TSI SMPS 3034 (scanning mobility particle sizer; Table 1; Lupi et al., 2016). The measurements were made between February and October in each year. Each scan over the particle size range takes 10 min, and we used 1-hr averages in this study. A side-by-side comparison with the DMPS measurements at the Mount Zeppelin Observatory was made by deploying the SMPS at Zeppelin in the spring of 2013, and good agreement (within 14%) was found (Lupi et al., 2016).

Figure 4 shows a scatter plot of the two aerosol measurement data sets obtained at the top (Zeppelin) and base (Gruvebadet) of the mountain using all of the 1-hr average data obtained between October 2013 and December 2015. In this figure, the integrated number concentrations of aerosols with dry diameters greater than 70 nm (hereafter denoted as  $N_{70}$ ) are compared. The dry diameter of 70 nm was adopted in this study because it is close to the median threshold diameter of aerosol activation,  $D_{\text{act}}$ , where  $D_{\text{act}}$  is defined as the diameter at which the integrated aerosol number concentration (greater than this diameter) becomes equal to  $N_c$  for clouds observed with temperatures warmer than 0 °C (section 3.3). Consequently,  $N_{70}$  is considered to be a proxy for the CCN concentrations under typical atmospheric conditions. Figure 4a shows the results when there were no clouds (i.e., no in-cloud data were measured within a 1-hr time period) at Zeppelin, while Figure 4b shows those obtained when in-cloud data were obtained at Zeppelin. No information is available on the presence of fogs at the Gruvebadet Observatory (mountain base). Both figures show that, in general, there is a good agreement between the  $N_{70}$  values, especially when there were no clouds. The

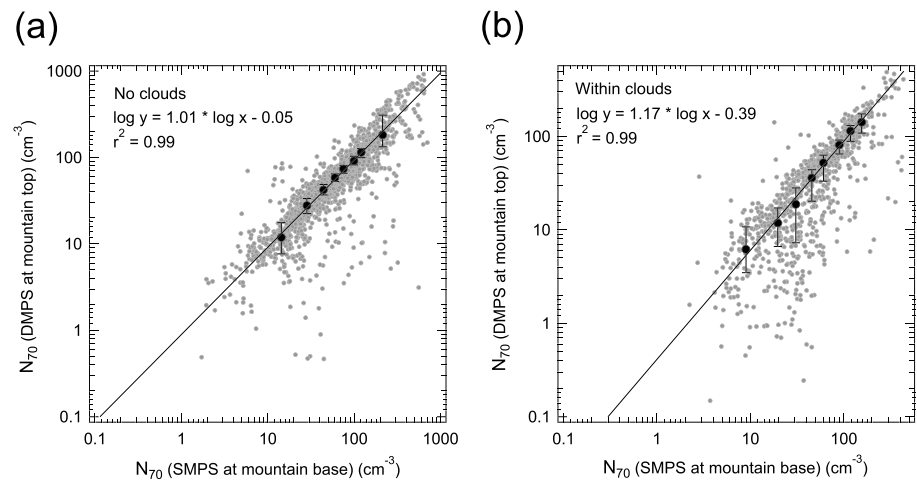


**Figure 4.** A scatter plot between the two aerosol measurements obtained at the top (Zeppelin Observatory, DMPS) and base (Grubebadet observatory, SMPS) of the mountain using all of the 1-hr average data obtained between October 2013 and December 2015. The integrated number concentrations of the aerosols with dry diameters greater than 70 nm ( $N_{70}$ ) are compared. (a) Results obtained when there were no clouds at Zeppelin. (b) Results when the “in-cloud” data were obtained at Zeppelin. Black closed circles and vertical bars indicate the median values and the 25th–75th percentiles, respectively, within the individual data ranges in which a similar number of data were obtained. Linear slopes and  $r^2$  values were calculated on the log of the values. DMPS = differential mobility particle sizer; SMPS = scanning mobility particle sizer.

slope of the log-log plot of the median values of the individual data ranges (black circles in Figure 4a) was close to unity. When different threshold diameters are adopted (e.g.,  $D > 40$  or 100 nm), similar degrees of agreement were found. For in-cloud conditions, on the other hand, the DMPS-derived  $N_{70}$  values were occasionally lower. These lower DMPS values could be real if air sampled at the top and base of the mountain had different air mass histories when clouds appeared at Mount Zeppelin and/or the precipitation removed aerosols within the upper layer. However, most of the observed lower  $N_{70}$  values were likely due to incomplete sampling and/or losses of the cloud particles within the whole air inlet used with the DMPS as described in Appendix C. Detailed analyses show that because of the dominance of small-size cloud particles ( $N_{c,r > 12.5\mu\text{m}}/N_c < 0.2$  for 90% of the data), the particle losses were likely less than 20% (Appendix C). Consequently, we have not made any corrections to the data and have not rejected any data in this study.

From the good agreement between the two aerosol measurements, we draw the following conclusions. First, the two measurements are consistent and only have small biases in concentrations. Second, the aerosol population is generally homogenous over the altitude range from the base of the mountain to its peak (up to approximately 500 m asl). A previous case study using aerosol lidar observations in Ny-Ålesund showed that the height of the planetary boundary layer was between 300 and 800 m (Di Liberto et al., 2012). The results obtained in this study suggest that even when the height of the planetary boundary layer is lower than the altitude of the Zeppelin Observatory, the large-scale transport of air with a relatively homogeneous distribution of aerosol particles at the lowest altitudes was likely responsible for the observed similarities in the aerosol concentrations. Finally, the agreement between the two measurements in the presence of clouds indicates that the aerosols within the cloud particles were successfully measured using the whole air inlet system, although errors became significant when large cloud particles were present (Appendix C). Consequently, we can directly compare the  $N_{70}$  values obtained at both observatories with  $N_c$  in the following analyses.

### 2.5. Other Measurements

The vertical profiles of the depolarization ratios of the cloud particles were measured using a micropulse lidar instrument (at the AWI or Rabben Observatories, before and after March 2015, respectively, Table 1 and Figure 1b). Data were recorded every 1 min, and 5-min average values were used in this study. The altitude resolution is 30 m, and values at 450, 480, and 510 m were used to estimate the phases of the cloud

particles observed at Zeppelin (474 m asl). Cloud layers were identified from the vertical profile of the attenuated backscatter ( $\Gamma > 2 \times 10^{-5} \text{ km}^{-1} \cdot \text{sr}^{-1}$ ; Sugimoto et al., 2001). When single scattering is assumed, depolarization ratios close to 0 indicate that the particles are spherical (i.e., water droplets), while large values indicate that particles are nonspherical (i.e., ice particles). Threshold values of the depolarization ratios of 3–11% have been used to separate spherical and nonspherical particles in previous studies (de Boer et al., 2009; Intrieri et al., 2002; Shupe, 2007); in this study, we adopted a threshold value of 4.3%. This value was derived from the measurements of clouds that quite likely consisted of only water droplets.

The cloud base heights were estimated using ceilometer measurements (Vaisala, CL 51) made at the AWI Observatory in Ny-Ålesund, which is located 2.1 km in horizontal distance from the Zeppelin Observatory (Table 1 and Figure 1b; Maturilli & Ebell, 2018). In our analysis, we also used hourly meteorological data, namely, the air temperature and horizontal wind speed/direction data, obtained using a Vaisala instrument at the Mount Zeppelin Observatory (Table 1). This instrument is mounted to a mast and is located approximately 15 m above the ground. Three-dimensional wind speed and direction (1 Hz) have also been measured near the FM-120 (the height of the inlet was 1.4 m) using an ultrasonic anemometer (the height of the sensing volume was 2.3 m) since December 2014. As described in Appendix A, horizontal wind speeds measured with the ultrasonic anemometer (near the ground surface,  $U_{2.3}$ ) were systematically slower than those measured with the Vaisala instrument (higher altitude,  $U_{15}$ ), likely due to the friction of the ground surface.

### 3. Results

#### 3.1. Frequency of Cloud Detections

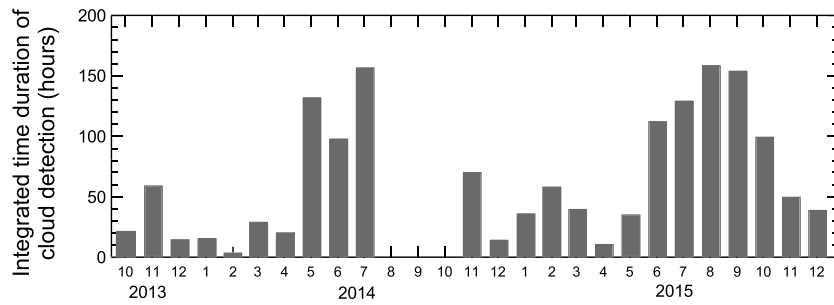
At the Mount Zeppelin Observatory, cloud measurements were made during 89% of the time period between October 2013 and December 2015 except for a period between August and October 2014 when no measurements were made due to building reconstruction. Figure 5 shows the integrated time durations during which in-cloud data were obtained for each month. The time durations were generally longer in summer. The durations ranged from 4 to 59 hr (on average, 26 hr a month or 3.6% of the time) between December and April, while the duration ranged from 130 to 159 hr (on average, 150 hr a month or 20.5% of the time) between July and September. Over the duration of the project, cloud data were obtained, on average, for 65 hr (8.9% of the time) during each month. The number of days when in-cloud data were obtained for more than 10 min ranged from 4 to 20 days (with an average value of 13.3 days) a month. A previous study using lidar measurements in Ny-Ålesund showed that the frequency of detection of the lowest-altitude clouds (with a cloud base height lower than 2 km) was higher between July and September compared with the rest of year (Shiobara et al., 2003).

In accordance with atmospheric temperatures (Figure 2), most clouds in July and August (82–93%) were detected when temperatures were higher than 0 °C, while most clouds between October and May (91–100%) were detected when temperatures were below 0 °C. In June and September, 14% to 45% of the cloud data were obtained at temperatures higher than 0 °C.

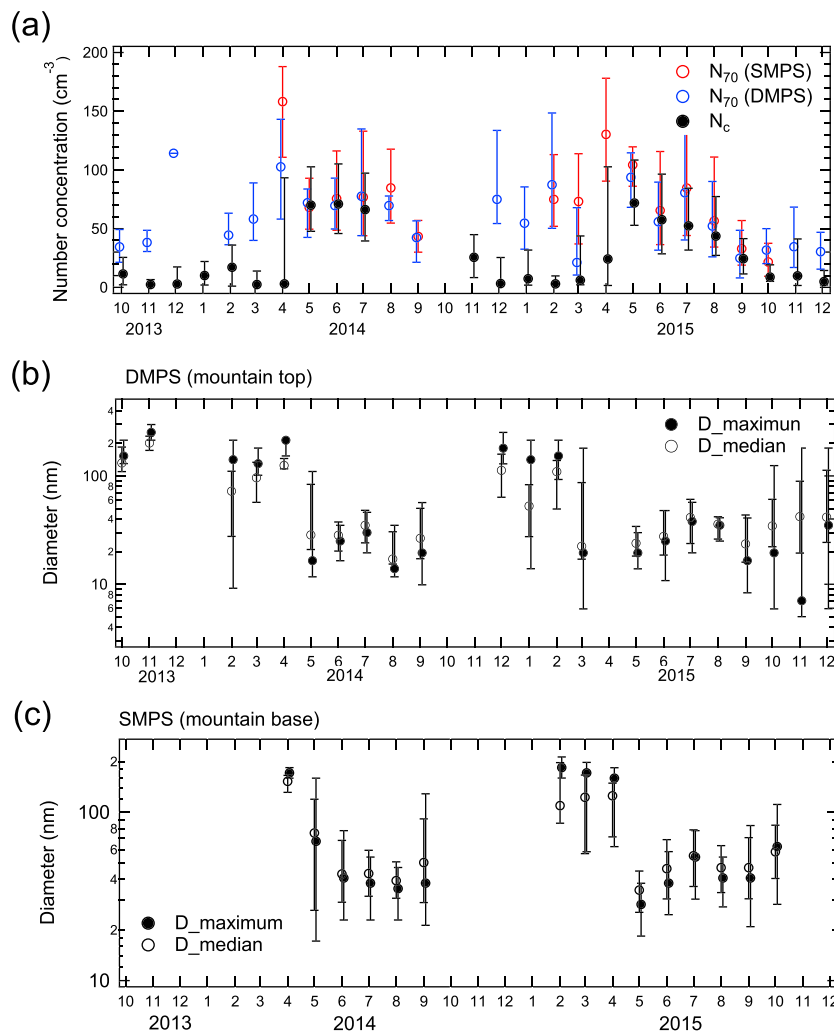
#### 3.2. Seasonal Variations in $N_c$ and Aerosol Size Distribution

Figure 6a shows the time series of the monthly median values of  $N_c$  and  $N_{70}$  for the time period between October 2013 and December 2015. The median  $N_c$  value reached its seasonal maximum in May–July ( $65 \pm 8 \text{ cm}^{-3}$ ), and it gradually decreased toward winter.  $N_c$  values were  $8 \pm 7 \text{ cm}^{-3}$  between October and March. A sharp increase in  $N_c$  occurred from March to May. This seasonal variation in  $N_c$  generally followed that of  $N_{70}$  observed at both Zeppelin (mountaintop) and Gruebadet (base), although  $N_c$  values were systematically lower than the  $N_{70}$  values between December and April. The similarities and differences in the seasonal variations of  $N_c$  and  $N_{70}$  are described later in terms of their correlations (sections 3.4–3.6).

Previous studies have suggested that aerosols are generally affected by anthropogenic emissions (Arctic haze) and new particle formation during the periods of March–May and June–August, respectively (Engvall et al., 2008; Strom et al., 2003; Tunved et al., 2013). Figures 6b and 6c show a time series of the median diameter of aerosol size distributions, where the integrated aerosol number concentrations greater and smaller than this diameter are equal. The diameters of the maximum concentration of aerosol size distributions ( $dN_a/d\log D$ ) are also shown. Although there are large variabilities in these diameters, they were generally greater than 100 nm (accumulation mode) between November and April, while they were smaller



**Figure 5.** An integrated time duration in which “in-cloud” data were obtained at the Zeppelin Observatory during each month. No data were obtained between August and October 2014 due to construction of the observatory.



**Figure 6.** (a) A time series of the monthly median values of the  $N_c$  and  $N_{70}$  data. Vertical bars indicate the 25th–75th percentiles. No cloud data were obtained between August and October 2014 due to construction of the observatory. (b) A time series of the monthly median values of the median diameter of aerosol size distribution, where the integrated aerosol number concentrations greater and smaller than this diameter are equal (open circles) for the DMPS (mountaintop) measurements. The diameters of the maximum concentration of aerosol size distributions ( $dN_a/d\log D$ ) are also shown (closed circles). Vertical bars indicate the 25th–75th percentiles. (c) Same as (b) but for the SMPS (mountain base) aerosol measurements. DMPS = differential mobility particle sizer; SMPS = scanning mobility particle sizer.

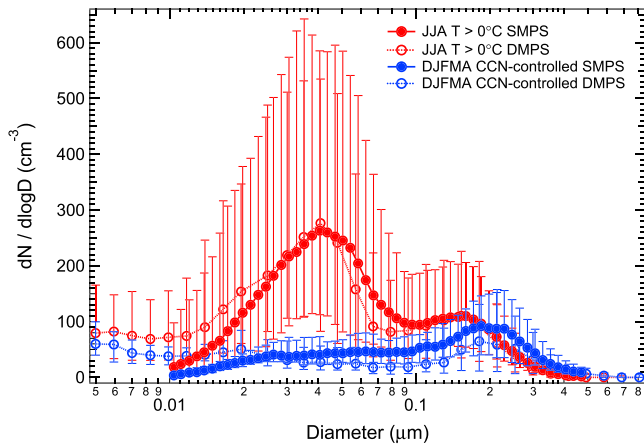


**Figure 7.** Aerosol size distribution (median values and 25th–75th percentiles) in summer (JJA,  $T > 0^\circ\text{C}$ ) and winter–spring (DJFMA, CCN-controlled data). JJA = June–August; DJFMA = December–April; CCN = cloud condensation nuclei; DMPS = differential mobility particle sizer; SMPS = scanning mobility particle sizer.

than 60 nm (Aitken mode) between May and October. Figure 7 shows aerosol size distributions (median values) for summer (June–August,  $T > 0^\circ\text{C}$ ) and winter–spring (December–April) seasons. For the winter–spring aerosol plot, we used only aerosol data, which show a positive correlation between  $N_c$  and  $N_{70}$  (the CCN-controlled data described in sections 3.4 and 3.5). The winter–spring aerosol data show maximum concentrations at approximately  $D = 200$  nm, and these accumulation-mode particles are likely due to the influences from anthropogenic emissions (Arctic haze). The summer aerosol data show bimodal distributions with maxima of approximately  $D = 40$  and 160 nm. The enhancement in the Aitken mode was likely due to the new particle formation (Tunved et al., 2013), although primary sea spray aerosols could also contribute to the formation of this aerosol mode (e.g., Quinn et al., 2015).

### 3.3. Activation Diameter, $D_{\text{act}}$ , for the Warm Clouds

Figure 8 shows the scatter plot of  $N_{70}$  and the threshold diameter of aerosol activation,  $D_{\text{act}}$  (the integrated aerosol number concentration greater than this diameter is equal to  $N_c$ ), using 1-hr data obtained with  $T > 0^\circ\text{C}$ . In this figure the median  $D_{\text{act}}$  values for individual  $N_{70}$  data ranges are also shown. Although there is a large dispersion of the  $D_{\text{act}}$

values for the given  $N_{70}$  values, the median  $D_{\text{act}}$  values decreased with decreasing  $N_{70}$  values, indicating that smaller aerosols were activated when the aerosol concentrations ( $N_{70}$ ) were lower. Similar tendencies were previously observed in low-level stratus in the subtropics (e.g., Hudson et al., 2010). The tendency observed in this study can be the result of various cloud microphysical/dynamical processes as well as aerosol chemical compositions/size distributions that depend on the aerosol concentrations. One of the possible explanations is that the maximum supersaturation ( $S_{\text{max}}$ ) that an air parcel experiences to form clouds tends to be higher when the number of activated aerosols is lower due to a lower condensation rate of the water vapor onto the cloud droplets (a lower condensation sink), leading to a smaller  $D_{\text{act}}$ . When the dependence of the CCN concentration ( $N_{\text{CCN}}$ ) on supersaturation ( $S$ ) is approximated as  $N_{\text{CCN}} = C S^k$  (where  $C$  is a CCN concentration for  $S = 1\%$  and  $k$  represents the size dependence of aerosols and ranges between 0.2 and 2.0), the dependence of  $S_{\text{max}}$  and resulting  $N_c$  on the CCN concentration ( $C$ ) can be approximated using a vertical wind velocity ( $w$ ) in clouds as follows (Rogers & Yau, 1989; Twomey, 1959):

$$S_{\text{max}} \propto \left( C^{-1} \cdot w^{\frac{3}{2}} \right)^{\frac{1}{k+2}} \quad (2)$$

$$N_c \propto \left( C^2 \cdot w^{\frac{3k}{2}} \right)^{\frac{1}{k+2}} \quad (3)$$

This well-known mechanism is denoted the “high- $S_{\text{max}}$  for low- $N_{\text{CCN}}$ ” mechanism, hereafter. In fact, as discussed in section 4, the simple air parcel model (the box model) calculations, which include this mechanism, can result in  $D_{\text{act}}$  to  $N_{70}$  relationships that are similar to those shown in Figure 8. In addition, very low CCN concentrations can induce fast droplet coalescence, which removes droplet surface area for condensational growth, and this process further increases supersaturation in clouds (Fan et al., 2018).

The median  $D_{\text{act}}$  values for all of the 1-hr data ( $T > 0^\circ\text{C}$ ) were 72.8 and 52.0 nm for the SMPS and DMPS measurements, respectively. When the  $N_{70}$  values were less than  $30 \text{ cm}^{-3}$ , aerosols with diameters down to 30–50 nm were activated as cloud droplets. These aerosols in summer are largely affected by new particle formation (Engvall et al., 2008; Strom et al., 2003; Tunved et al., 2013). Although these aerosols are generally too small to act as CCN for low-level clouds, they likely play important roles in the Arctic. The activation of small aerosols ( $D < 50$  nm) was also suggested in other low-aerosol regions, such as in the pristine Amazon region (e.g., Fan et al., 2018). Notably, the entrainment of cloud free air into cloudy air after aerosol activation can reduce  $N_c$ . Consequently,  $D_{\text{act}}$  can be even lower than the estimates shown here.

In this study, we adopted a threshold diameter of 70 nm to estimate CCN because it is close to the median  $D_{\text{act}}$  values and because a high correlation coefficient between  $N_c$  and  $N_{70}$  was found (section 3.4).

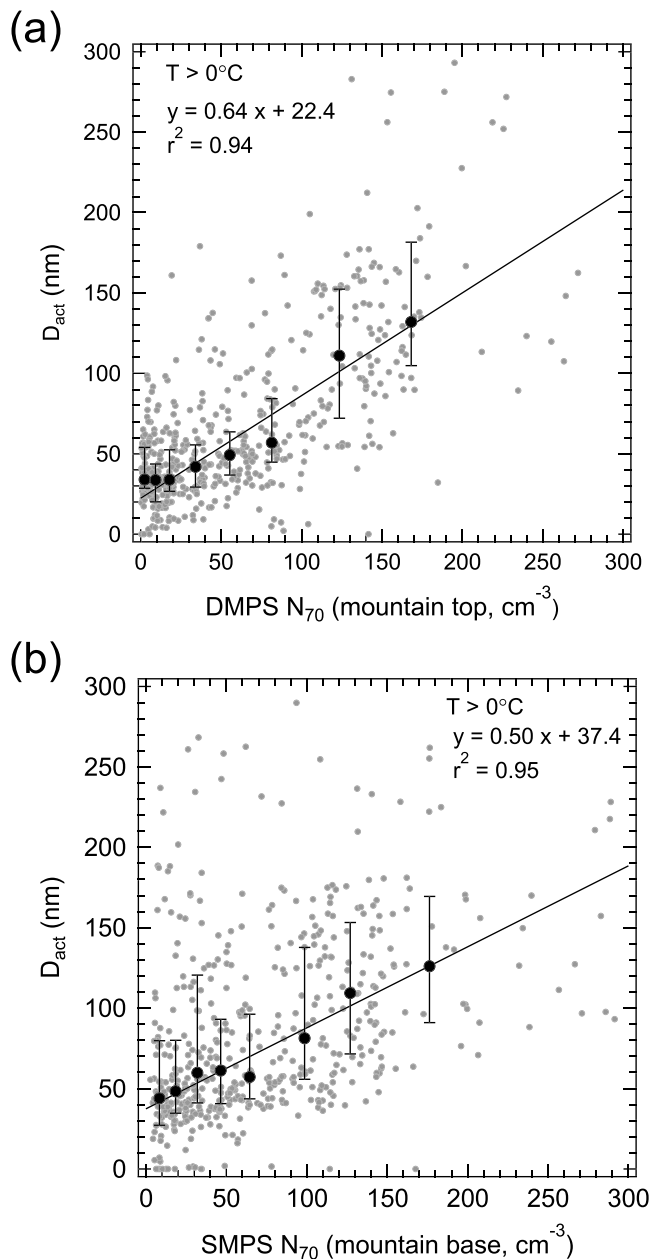


**Figure 8.** A scatter plot between  $N_{70}$  and  $D_{act}$  (the integrated aerosol number concentration greater than this diameter is equal to  $N_c$ ) using all of the 1-hr data obtained with  $T > 0^\circ\text{C}$ . (a) DMPS-derived  $N_{70}$  (mountain top) and (b) SMPS-derived  $N_{70}$  (mountain base) are used. Black circles and vertical bars indicate median values and 25th–75th percentiles, respectively. They are calculated within individual data ranges, in which a similar number of data were obtained. Linear slopes and  $r^2$  values for these median values are given. DMPS = differential mobility particle sizer; SMPS = scanning mobility particle sizer.

The results presented in this study are essentially the same when slightly different threshold values are used to estimate the CCN concentrations.

### 3.4. Relationship Between $N_{70}$ and $N_c$ in Summer ( $T > 0^\circ\text{C}$ )

Figures 9a and 9b show the scatter plots between  $N_c$  and  $N_{70}$  (mountain-top DMPS and mountain base SMPS, respectively) using all of the 1-hr data. The color denotes the atmospheric temperature at Zeppelin. These figures show that both the  $N_{70}$  and  $N_c$  values vary over more than 2 orders of magnitude. In each figure, the data can be classified into two distinct groups. One of the groups shows a clear positive relationship, suggesting that  $N_c$  is generally controlled by the CCN concentrations (CCN-controlled data). All of the data obtained at temperatures warmer than  $0^\circ\text{C}$  and some of the data obtained at temperatures below  $0^\circ\text{C}$  belong to this group. On the other hand, some of the data obtained at temperatures below  $0^\circ\text{C}$  show systematically lower  $N_c$  values than the data obtained above  $0^\circ\text{C}$ , and they exhibit little or no correlation with  $N_{70}$  (CCN-uncontrolled data). In this section, we describe the data obtained for temperatures  $\geq 0^\circ\text{C}$ , while the data obtained below  $0^\circ\text{C}$  are described in the following section.

The black circles in Figures 9a and 9b show the median  $N_c$  values within individual  $N_{70}$  ranges for the data obtained above  $0^\circ\text{C}$ . As previously defined in equation (1), one third of the slope of the relationship between  $\log N_c$  and  $\log N_{70}$  ( $1/3 \Delta \log N_c / \Delta \log N_{70}$ ) corresponds to the ACI index. From the curve fits on the data shown in Figures 9a and 9b, the index values of 0.18 and 0.21 were derived for the DMPS and SMPS median data, respectively, between June and August (Table 2). When the two largest median  $N_{70}$  values are excluded (using six median values instead of using eight), the ACI index values increase to 0.23 and 0.25, and the correlation coefficients ( $r^2$ ) also increase. These slight increases are because the relatively low  $N_c$  values at the highest  $N_{70}$  values are excluded. From these estimates, the average ACI index in summer (June–August,  $T > 0^\circ\text{C}$ ) was calculated to be  $0.22 \pm 0.03$  (Table 2). The high sensitivity of the cloud microphysics to changes in the aerosol concentration underscores the importance of understanding the sources and behaviors of aerosols in the Arctic.

The reason for the relatively low  $N_c$  values at the highest  $N_{70}$  values is not clear. The air parcel model calculations described in section 4 did not show these tendencies: The model-calculated  $N_c$  increases with increasing  $N_{70}$  within the  $N_{70}$  range examined here. One possible cause of the low  $N_c$  values is changes in updraft velocity (Appendix A); however, detailed analyses need to be conducted in a future study. Notably, even when the ACI index is calculated using only the data from individual ranges of precipitation rates, namely,  $<0.01$ ,  $0.01$ – $1.0$ , and  $>1.0$  mm/day, no systematic changes were found, although the  $N_{70}$  and  $N_c$  data ranges were lower for higher precipitation rates, likely due to the wet removal of aerosols by precipitation. The relatively low  $N_c$  values at the highest  $N_{70}$  values do not necessarily correspond to higher precipitation rates. These results

indicate that although precipitation can change the absolute values of  $N_{70}$  and  $N_c$  through cloud microphysical processes (e.g., accretion and wet removal of aerosols) and dynamical processes (e.g., changes in heating/cooling rates and turbulent kinetic energy), the CCN control of  $N_c$  generally keeps the slope of the  $N_c$  to  $N_{70}$  relationship fixed under various meteorological conditions.

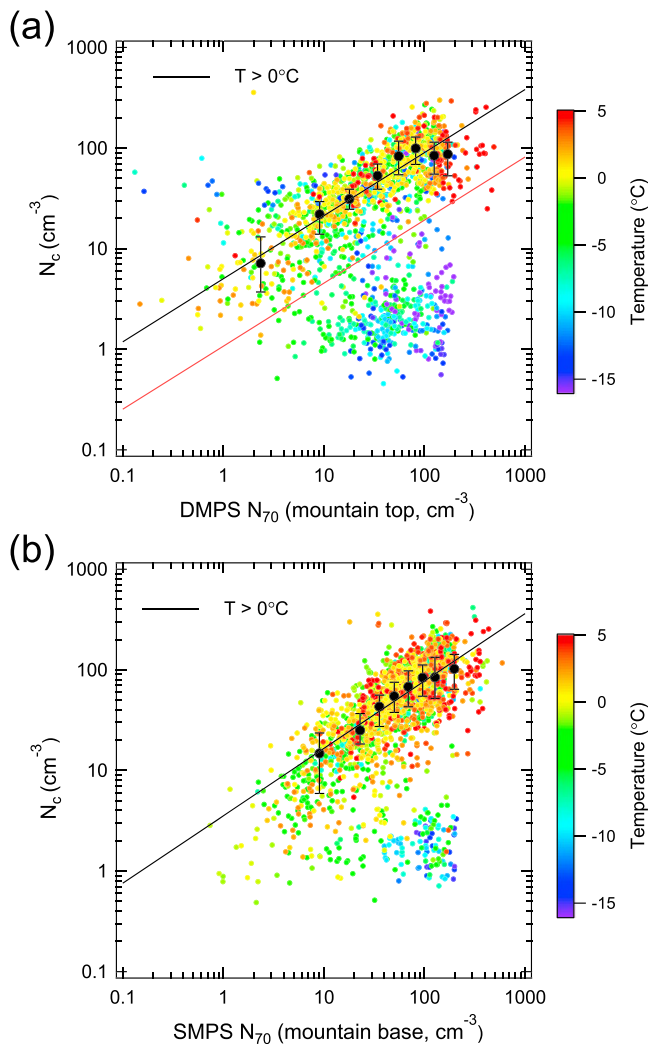


**Figure 9.** A scatter plot of one-hour data between  $N_{70}$  and  $N_c$ . (a) DMPS-derived  $N_{70}$  (mountaintop) and (b) SMPS-derived  $N_{70}$  (mountain base) are used. Colors of the data points indicate the temperature at the Zeppelin Observatory. Black circles and vertical bars indicate median values and 25th–75th percentiles, respectively, for data obtained with  $T > 0^\circ\text{C}$ . They are calculated within the individual data ranges, in which a similar number of data were obtained. The red line in (a) denotes the threshold values used to separate the “CCN-controlled” and “CCN-uncontrolled” data sets (above and below this line, respectively). DMPS = differential mobility particle sizer; SMPS = scanning mobility particle sizer; CCN = cloud condensation nuclei.

situ measurements in the Pallas area of northern Finland ( $68^\circ\text{N}$ ,  $24^\circ\text{E}$ ; Lihavainen et al., 2010). The systematic differences in the ACI index estimates between in situ and satellite measurements are consistent with previous studies (e.g., McComiskey & Feingold, 2012), and the estimates obtained from in situ measurements in this study are considered to be much more robust.

### 3.5. Relationship Between $N_{70}$ and $N_c$ at $T < 0^\circ\text{C}$

The scatter plots between  $N_{70}$  and  $N_c$  (Figure 9) show that the data obtained at temperatures below  $0^\circ\text{C}$  can be classified into two groups: Some points lie along the summertime  $N_c$  to  $N_{70}$  relationship, while others show systematically lower  $N_c$  values. The former and the latter groups are hereafter denoted as the “CCN-controlled” and the “CCN-uncontrolled” data sets, respectively (above and below the red line in Figure 9a). Figures 10a and 10b show histograms of the depolarization ratios at altitudes of 450, 480, and

ACI index values  $< 0.33$  indicate that the rate of increase in  $N_c$  is less than that of  $N_{70}$ , namely,  $(d\ln N_c)/(d\ln N_{70}) < 1$ . As described in the previous section,  $D_{\text{act}}$  generally increases as  $N_{70}$  increases (Figure 8). This tendency corresponds to a lower rate of increase in  $N_c$  than in  $N_{70}$ , as shown in Figure 9. In fact, if  $D_{\text{act}}$  does not change with  $N_{70}$ , (and everything else also does not change),  $d\ln N_c/d\ln N_{70}$  achieves unity. The observed  $D_{\text{act}}$  to  $N_{70}$  relationships and  $N_c$  to  $N_{70}$  relationships (therefore, the ACI index values) can be the result of various factors/mechanisms; however, as previously discussed, the simple high- $S_{\text{max}}$  for low- $N_{\text{CCN}}$  mechanism is one of the possible explanations. In fact, as described later (section 4), the air parcel model calculations, which include this mechanism, can reproduce the observed tendencies.

Lihavainen et al. (2010) argued that the ACI index estimates can change depending on the definition of the aerosol burden, namely, a choice of the threshold diameter ( $D_{\text{threshold}}$ ), for which the integrated aerosol number concentration greater than this diameter is calculated. When the ACI index was calculated in this study for various  $D_{\text{threshold}}$  values (various aerosol concentrations), the ACI index estimates changed. With increasing  $D_{\text{threshold}}$  values, the ACI index values generally decrease when the DMPS data are used, while the ACI index values show a broad maximum at  $D_{\text{threshold}}$  values of approximately 70 nm when the SMPS data are used (not shown). In addition, the correlation coefficients between  $N_c$  and aerosol concentrations become lower when  $D_{\text{threshold}}$  values lower than approximately 70 nm are used. The use of  $N_{70}$  for the ACI analyses in this study is reasonable because this diameter is close to the median  $D_{\text{act}}$  value (72.8 and 52.0 nm for SMPS and DMPS measurements, respectively). The CCN concentrations should be used to estimate aerosol impacts on water clouds.

The ACI index values can also be estimated from the relationships between  $N_{70}$  and the cloud effective radius ( $r_e$ ). Because  $r_e$  depends on both  $N_c$  and CWC, the ACI index values were individually calculated for six ranges of CWC values. As a result, ACI index values of  $0.24 \pm 0.04$  were obtained ( $T > 0^\circ\text{C}$ ). These values are in accordance with the estimates derived from the relationships between  $N_c$  and  $N_{70}$  ( $0.22 \pm 0.03$ ).

Previous estimates of the ACI index values in the Arctic ranged between 0.0 and 0.19 when remote sensing data or limited aircraft in situ data were used (Coopman et al., 2016; Garrett et al., 2004; Tietze et al., 2011; Zamora et al., 2016), although values close to 0.33 were derived in limited cases (Coopman et al., 2018). Compared with these estimates, the values of 0.22–0.24 obtained in this study are systematically higher and are generally in agreement with those of 0.2–0.3 obtained using ground-based in

**Table 2**  
Aerosol-Cloud Interaction (ACI) Index for CCN-Controlled Data

Season	ACI index ( $\text{dln}N_c/(3\text{dln}N_{70})$ ) and $r^2$		Number of 1-hr data
	Six median values	Eight median values	
Aerosol: mountain base (SMPS)			
Jun–Aug	0.23 (0.96)	0.20 (0.93)	602
Sep–Nov	0.27 (0.58)	0.24 (0.73)	207
Dec–Feb	0.37 (0.39)	0.25 (0.58)	16
Mar–May	0.25 (0.96)	0.25 (0.97)	140
Jun–Aug ( $T > 0^\circ\text{C}$ )	0.25 (0.99)	0.21 (0.95)	766
Dec–Apr	0.28 (0.96)	0.26 (0.96)	81
Aerosol: mountaintop (DMPS)			
Jun–Aug	0.22 (1.00)	0.18 (0.92)	602
Sep–Nov	0.14 (0.89)	0.18 (0.93)	332
Dec–Feb	0.27 (0.94)	0.26 (0.96)	189
Mar–May	0.17 (0.95)	0.16 (0.95)	140
Jun–Aug ( $T > 0^\circ\text{C}$ )	0.23 (0.99)	0.18 (0.89)	425
Dec–Apr	0.24 (0.94)	0.23 (0.96)	254

*Note.* ACI index values are calculated using the median values within the individual data ranges (in total, eight ranges). These values are also calculated by excluding the two largest median values of  $N_{70}$  (six median values), because slightly different tendencies were found, especially in summer ( $T > 0^\circ\text{C}$ ). Values in parentheses are correlation coefficients ( $r^2$  values). The ACI index value greater than 0.33 (0.37) was likely due to error in the curve fitting considering the low  $r^2$  value (0.39). CCN = cloud condensation nuclei; SMPS = scanning mobility particle sizer; DMPS = differential mobility particle sizer.

510 m measured by the micropulse lidar (section 2.5 and Table 1), when CCN-controlled and CCN-uncontrolled clouds, respectively, were observed at Zeppelin ( $T < 0^\circ\text{C}$ ). Five-minute lidar data were used. The vertical line (at the depolarization ratio of 0.043) represents the threshold value used to classify spherical (liquid droplets) and nonspherical (ice) particles in this study (section 2.5). This figure suggests that the CCN-controlled data were likely to be supercooled water droplets, while the CCN-uncontrolled data were likely to be obtained under the presence of ice particles. In the latter case (large depolarization ratios), liquid water droplets can still exist because ice particles mixed with water droplets can cause high depolarization ratios. Notably, that the coexistence of precipitating particles with cloud particles can affect the depolarization measurements. The colors of Figure 10 denote the number concentrations of the precipitating particles ( $r = 25\text{--}775\ \mu\text{m}$ ) measured with the MPS. In general, the precipitating particle number concentrations are higher when the CCN-uncontrolled data were obtained (note that different color scales are used for Figures 10a and 10b). If these precipitating particles are ice, then they could result in a higher depolarization ratio even when the cloud particles are liquid. However, even when no precipitating particles were observed ( $N = 0$  data denoted by the black color), high depolarization ratios were still observed for the CCN-uncontrolled data, thus suggesting the presence of ice cloud particles (nonprecipitating particles) whose radii are generally smaller than  $25\ \mu\text{m}$ .

The number concentrations of supercooled water droplets are considered to be controlled by the number concentrations of the CCN; therefore, it is reasonable that these CCN-controlled data follow the summertime  $N_c$  to  $N_{70}$  relationship. Furthermore, the median  $D_{\text{act}}$  values for all of the

CCN-controlled data (1-hr data including both  $T > 0^\circ\text{C}$  and  $< 0^\circ\text{C}$  data) were 70.4 and 48.0 nm for the SMPS and DMPS measurements, respectively, and these values are very close to the  $D_{\text{act}}$  values of 72.8 and 52.0 nm for data with  $T > 0^\circ\text{C}$ . These results suggest that clouds observed with  $T > 0^\circ\text{C}$  (mostly in summer) and CCN-controlled clouds (observed throughout the year) are generally similar in terms of their aerosol activation processes, although the aerosol size distributions in summer and winter-spring are systematically different (Figure 7).

Figure 11 compares the relationships of  $N_c$  to  $N_{70}$  for the CCN-controlled data between the summer (June–August) and winter–spring (December–April) seasons. The  $N_c/N_{70}$  ratios were slightly higher in summer, and they could be due to higher updraft velocities and/or more hygroscopic aerosols in summer. However, the slopes are generally similar between the two seasons. The ACI index values for the summer and winter–spring seasons (CCN-controlled data) were  $0.22 \pm 0.03$  and  $0.25 \pm 0.02$ , respectively (Table 2). Although the latter values are slightly higher, the uncertainty ranges of the two values overlap. Furthermore, when the ACI index values were calculated for the individual seasons, they did not show a clear seasonal variation (Table 2). Previous studies have suggested that aerosols are generally affected by anthropogenic emissions (Arctic haze) and new particle formation during the periods of March–May and June–August, respectively (Engvall et al., 2008; Strom et al., 2003; Tunved et al., 2013). The present results suggest that, in terms of the ACI index values, the aerosol impacts on the microphysics of liquid clouds are generally not very different between these two periods (two aerosol sources).

Regarding the CCN-uncontrolled data, the  $N_c$  values are generally between  $0.8$  and  $5\ \text{cm}^{-3}$ , and they are lower than the CCN-controlled data by a factor of more than 10 when data with similar  $N_{70}$  values are compared (Figure 9). These low  $N_c$  values are considered to be consistent with the fact that CCN-uncontrolled clouds likely contain ice particles (Figure 10): The INP concentrations are generally much lower than the CCN concentrations, and the Bergeron-Findeisen process tends to reduce  $N_c$ . However, these observed  $N_c$  values are much higher than the typical ice particle concentrations previously observed in Arctic clouds (e.g., McFarquhar et al., 2011; Verlinde et al., 2007). Because not all particles of the CCN-uncontrolled

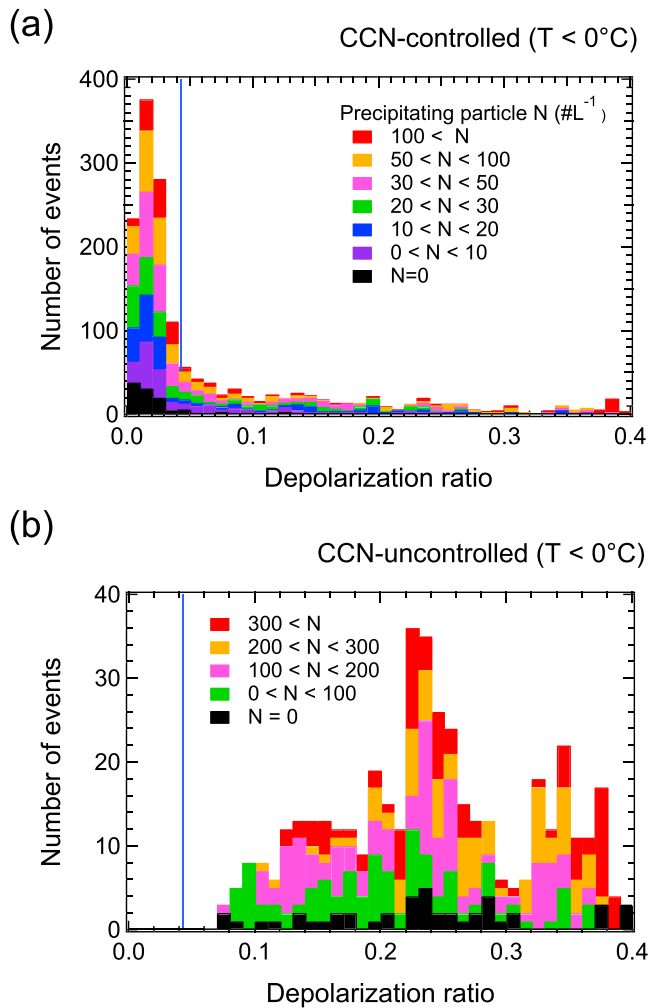


**Figure 10.** A histogram of the depolarization ratios at altitudes of 450, 480, and 510 m measured by the micropulse lidar (at the AWI or Rabben Observatories, before and after March 2015, respectively; Table 1 and Figure 1b) when (a) CCN-controlled and (b) CCN-uncontrolled clouds were observed at Zeppelin ( $T < 0^\circ\text{C}$ ). Five-minute lidar data were used. The vertical line (a depolarization ratio of 0.043) indicates the threshold value used to distinguish spherical (liquid droplets) and nonspherical (ice) particles in this study (section 2.5). The colors denote the number concentrations of the precipitating particles ( $r = 25\text{--}775\ \mu\text{m}$ ) measured by the MPS. Note that different color scales are used for a and b. AWI = Alfred Wegener Institute; CCN = cloud condensation nuclei; MPS = Meteorological Particle Sensor.

number of data points. The  $N_c$  values ranged from 21 to  $67\ \text{cm}^{-3}$  throughout the year, and these relatively high  $N_c$  values in the winter are considered to be partly sustained by the long-range transport of anthropogenic aerosols (Arctic haze).

Figure 14b shows that the CWC values of the CCN-controlled data are systematically higher in summer (June–August) than in the autumn and early winter months (October–December). The CWC value in July is a factor of 3.3 times greater than that in December. The summertime atmosphere can hold more moisture due to its higher temperature (Clausius-Clapeyron equation); therefore, the CWC is generally higher. This thermodynamic effect was estimated by calculating the moist adiabatic condensation coefficient (adiabatic CWC lapse rate,  $C_w$ ). The results indicate that  $C_w$  was greater by a factor of only 1.8 at  $4^\circ\text{C}$  than at

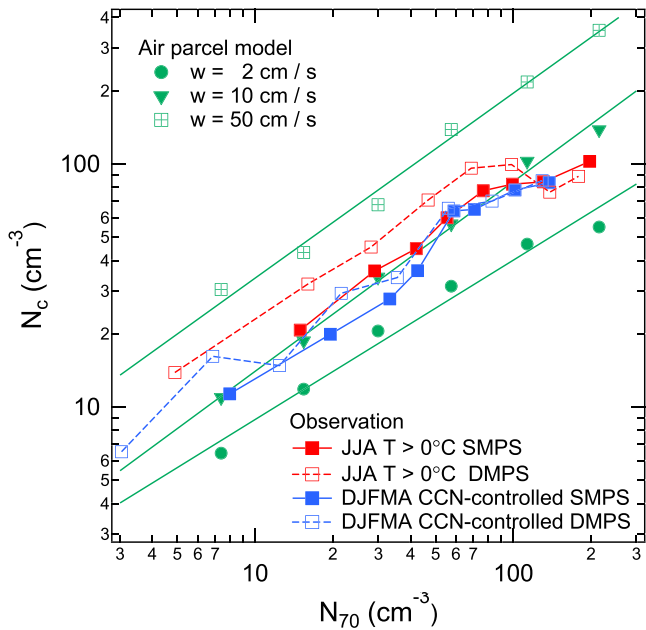
clouds were necessarily ice particles in our measurements, they might not be comparable with previous reports of ice particle concentrations. The systematic differences are also partly because ice particles were identified only for precipitating particle sizes (e.g.,  $r > 50\ \mu\text{m}$ ) in some of the previous studies, while both liquid droplets and ice particles with  $r < 23.5\ \mu\text{m}$  were measured together to obtain the  $N_c$  values in this study. We also note that the definition of “in-cloud data” can affect the average/median calculations. We used only in-cloud data, which is defined as having CWC values greater than  $0.01\ \text{g/m}^3$  (section 2.2), to calculate  $N_c$ . This CWC value corresponds to  $N_c = 2.4\ \text{cm}^{-3}$ , when all of the cloud particles have  $r = 10\ \mu\text{m}$ . If we adopt lower CWC or  $N_c$  threshold values, the average  $N_c$  value decreases.

Figure 12 shows that the fraction of CCN-uncontrolled data increased with decreasing temperature. At temperatures higher than  $-4^\circ\text{C}$ , the CCN-uncontrolled data fraction was low (less than 20%), while at temperatures between  $-4$  and  $-19^\circ\text{C}$ , the CCN-uncontrolled data fraction was approximately 50%. When the temperature was lower than  $-19^\circ\text{C}$ , this fraction reached 100%. This tendency is generally consistent with the presence of ice particles observed in the Arctic from aircraft (e.g., Gayet et al., 2009) and the ground (e.g., Shupe, 2011), although the cloud top temperature was incorporated in the former study. The temperature dependence of the presence of ice particles is partly controlled by the presence of INP and CCN concentrations. The interpretations of ice particle concentrations and their temperature dependence are currently being studied and will be presented in another paper.

### 3.6. Seasonal Variation of $r_e$ and CWC

Figure 13 shows the time duration fractions of cloud detection with  $T > 0^\circ\text{C}$ ,  $T < 0^\circ\text{C}$  (CCN-controlled), and  $T < 0^\circ\text{C}$  (CCN-uncontrolled). This figure shows that although the period when the atmospheric temperature was higher than  $0^\circ\text{C}$  was short at Zeppelin, CCN-controlled data (water droplets) persistently appeared throughout the year. This result indicates that the CCN concentrations play an important role in controlling the cloud microphysics that affect the radiative properties of the clouds and their various indirect effects.

Figures 14a–14c show the seasonal variations in the monthly median values of  $N_c$ , CWC, and  $r_e$ . In these figures, the values for the CCN-controlled data (both  $T > 0^\circ\text{C}$  and  $T < 0^\circ\text{C}$  data) and CCN-uncontrolled data are shown separately. All 3 years of data are used. The CCN-controlled data (likely to be liquid water clouds) are examined first. As expected from the definition of the CCN-controlled data, the  $N_c$  values generally follow the  $N_{70}$  values, although some deviations were found in winter months, likely due to the statistical fluctuations related to the small



**Figure 11.** Observed and model-calculated relationships between  $N_{70}$  and  $N_c$ . For the observations, the median  $N_c$  values for the individual  $N_{70}$  ranges are shown for the two seasonal periods (JJA and DJFMA) and two aerosol measurement instruments (SMPS and DMPS). Air parcel model calculations shown here were made for individual  $N_{70}$  ranges using the SMPS-derived aerosol data (JJA and  $T > 0^\circ\text{C}$ ) as inputs. The ACI index values defined in equation (1) were calculated from these observed slopes ( $\text{dlog}N_c / (3\text{dlog}N_{70})$ ) and are given in Table 2. JJA = June–August; DJFMA = December–April; DMPS = differential mobility particle sizer; SMPS = scanning mobility particle sizer; ACI = aerosol–cloud interaction; CCN = cloud condensation nuclei.

$-11^\circ\text{C}$  (typical temperatures during summer and winter months, respectively). Consequently, this effect alone may not explain the observed amplitude of the seasonal variations in the CWC values. Several other factors, such as the seasonal variations in the cloud base height and the entrainment rate of dry air, could also have contributed to the seasonal variations. It is beyond the scope of this study to examine these factors; however, the microphysical properties of clouds measured by in situ measurements should also be studied from the viewpoint of the vertical structure of the clouds.

Because both the  $N_c$  and CWC values of the CCN-controlled data are generally higher in summer,  $r_e$  values do not show clear seasonal dependence, and they were between  $5.7$  and  $9.2\ \mu\text{m}$  throughout the year (Figure 14c). With these small  $r_e$  values, the emissivity of cloud particles depends on the particle radius, although emissivity is less sensitive to the particle radius for  $r_e > 10\ \mu\text{m}$ . Consequently, changes in the CCN concentration, which leads to changes in  $r_e$ , could affect the longwave radiative forcing of the clouds (Lubin & Vogelmann, 2006).

Finally, the  $N_c$ , CWC, and  $r_e$  values of the CCN-uncontrolled data (clouds likely containing ice particles) are examined. The  $N_c$  values were mostly between  $1.6$  and  $2.9\ \text{cm}^{-3}$ , and clear seasonal variations could not be identified (Figure 14a). The CWC values were systematically lower than those of the CCN-controlled data. Because we assumed that cloud particles are spherical in the calculation of the CWC, we might be overestimating the CWC values when the CCN-uncontrolled data include many ice particles. The  $r_e$  values were between  $7.8$  and  $17.1\ \mu\text{m}$ , and these values were systematically greater than those for the CCN-controlled data (Figure 14c).

#### 4. Discussion

As described in section 3.3 (Figure 8), the median  $D_{\text{act}}$  values decrease with decreasing  $N_{70}$  values. Although this tendency can result from various processes, it is also in accordance with that expected from the high- $S_{\text{max}}$  for low- $N_{\text{CCN}}$  mechanism (section 3.3). To quantitatively examine this mechanism, air parcel model (the box model) calculations were performed using a simulation that calculates cloud particle formation from aerosols within an ascending air parcel by explicitly calculating supersaturation in the air (Feingold & Heymsfield, 1992). The aerosol size distributions used for these calculations were derived from the SMPS measurements (at the mountain base,  $T > 0^\circ\text{C}$ , June–August) for individual  $N_{70}$  ranges (the averages for each of the six ranges between  $5$  and  $320\ \text{cm}^{-3}$ , Table 3). The initial temperature, pressure, and relative humidity values for the parcel model calculations were also taken from observations

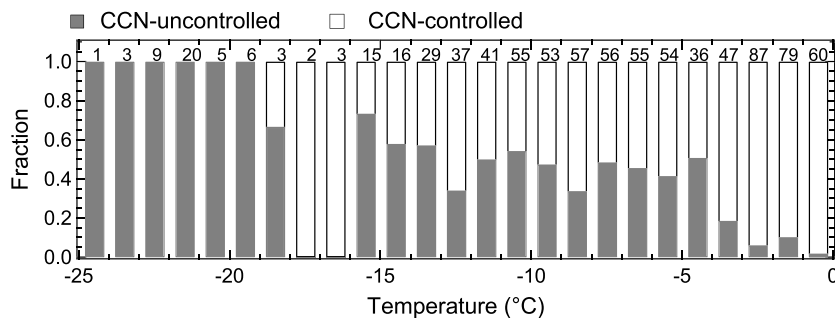


**Figure 12.** A fraction of the time duration of CCN-uncontrolled cloud detection (gray) as a function of the atmospheric temperature at Zeppelin (not cloud top temperature). The number of 1-hr data used for this statistical analysis is also shown. CCN = cloud condensation nuclei.

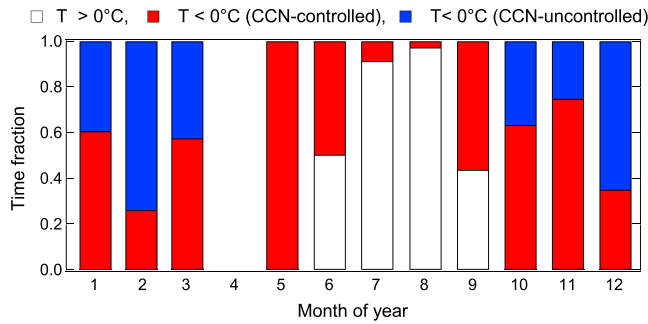


**Figure 13.** The fractions of the time duration of cloud detection at  $T > 0^\circ\text{C}$  (white), CCN-controlled cloud detection at  $T < 0^\circ\text{C}$  (red), and CCN-uncontrolled cloud detection at  $T < 0^\circ\text{C}$  (blue). No data are available for April because simultaneous collection of clouds, aerosols, and meteorological data did not occur. CCN = cloud condensation nuclei.

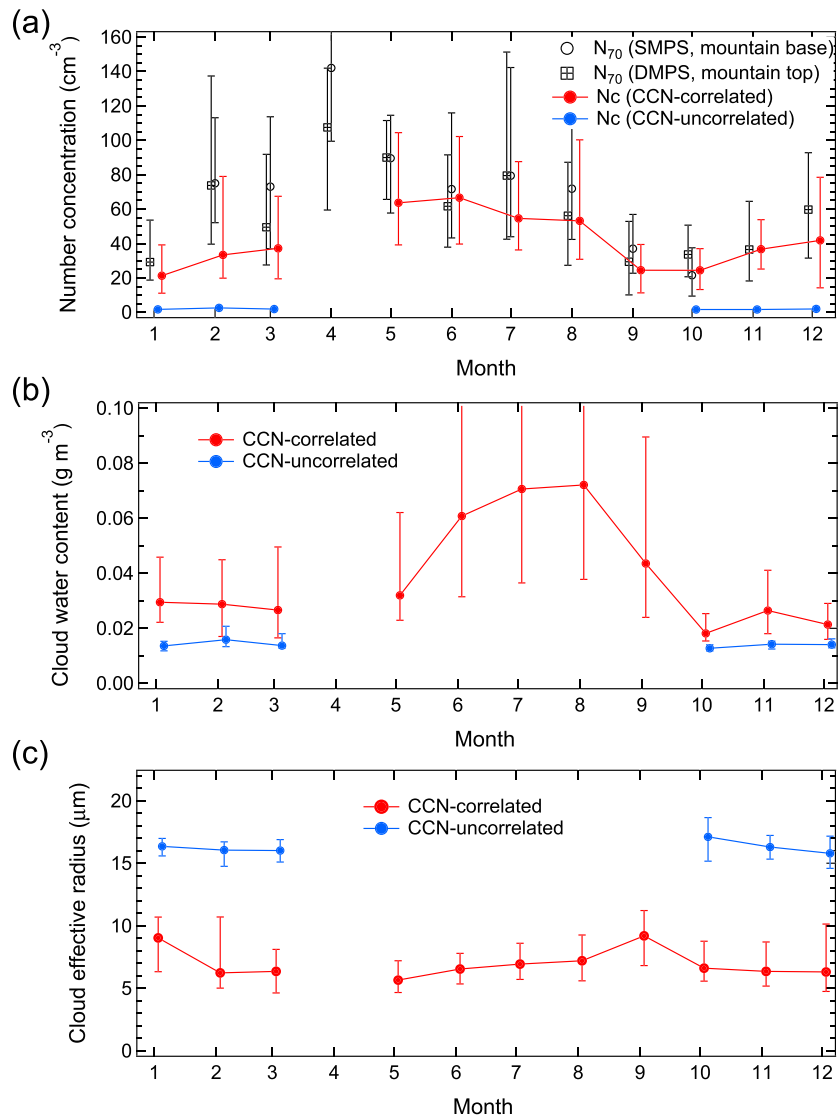
at Zeppelin, and common values ( $2.3^\circ\text{C}$ ,  $956.6\text{ hPa}$ , and  $92.6\%$ , respectively) were used for all of the calculations. For the chemical composition, we assumed ammonium sulfate ( $(\text{NH}_4)_2\text{SO}_4$ ) because secondary aerosols, including sulfate, were frequently observed at Zeppelin (Weinbruch et al., 2012). The calculations were performed for various updraft velocities (in  $1\text{-cm/s}$  increments), and we chose an updraft velocity that resulted in the best agreement with the observed  $N_c$  values (the averaged values for the individual  $N_{70}$  data ranges), hereafter referred to as the effective updraft velocity,  $W_{\text{eff}}$ . From each of these six sets of air parcel model calculations (the six ranges for the  $N_{70}$  values), the  $W_{\text{eff}}$ ,  $D_{\text{act}}$ , and maximum supersaturation ( $S_{\text{max}}$ ) values within the air parcels were obtained.

Table 3 shows the results of these calculations. Both the  $W_{\text{eff}}$  values between 6 and  $20\text{ cm/s}$  and the resulting  $S_{\text{max}}$  values of  $0.2\text{--}0.8\%$  are considered reasonable under moderate weather conditions, which produce persistent low-level clouds in Ny-Ålesund. Similar results were also

obtained when the DMPS aerosol data (the mountaintop) were used for the model inputs. In general, higher  $W_{\text{eff}}$  values were obtained for lower  $N_{70}$  values (Table 3). This dependence is realistic if lower aerosol concentrations were observed in association with higher vertical wind speeds. However, even when a constant vertical wind speed ( $10\text{ cm/s}$ ) is used for the air parcel calculations, the observed  $D_{\text{act}}$  dependence on  $N_{70}$  was generally reproduced (Table 3). We do not intend to argue that the observed  $D_{\text{act}}$  dependence on  $N_{70}$  is quantitatively explained solely by the high- $S_{\text{max}}$  for low- $N_{\text{CCN}}$  mechanism. Various parameters/processes, such as the dry air entrainment rate, can concurrently change with aerosol concentrations, and they can also affect the  $D_{\text{act}}$  to  $N_{70}$  relationship. Despite these uncertainties, the simple cloud microphysical mechanism of high- $S_{\text{max}}$  for low- $N_{\text{CCN}}$  can explain the relationships that have been observed in the measurements.

From a previous aircraft experiment over Resolute Bay ( $74\text{--}78^\circ\text{N}$ ) in summer, mean  $N_c$ ,  $S_{\text{max}}$ , and  $D_{\text{act}}$  values of  $10\text{--}100\text{ cm}^{-3}$ ,  $0.3\text{--}0.6\%$ , and  $50\text{ nm}$  were obtained, although  $D_{\text{act}}$  values as low as  $20\text{ nm}$  were suggested in specific cases (Leaith et al., 2016). These values are generally similar to those obtained in this study. Although not in the Arctic, at a site off the coast of California,  $S_{\text{max}}$  values of  $0.1\text{--}1\%$  were obtained with high CCN and  $N_c$  concentrations ( $100\text{--}300\text{ cm}^{-3}$ ) in low-level stratus (Hudson et al., 2010). Under even higher  $N_c$  conditions ( $1,460\text{ cm}^{-3}$  on average in near adiabatic updraft cores) observed in the low-level clouds over the east China Sea in spring, average values of  $D_{\text{act}}$ ,  $W_{\text{eff}}$ , and  $S_{\text{max}}$  of  $114\text{ nm}$ ,  $72\text{ cm/s}$ , and  $0.24\%$ , respectively, were estimated (Koike et al., 2012). Compared with the values obtained under Asian pollution conditions, the  $D_{\text{act}}$  and  $W_{\text{eff}}$  values obtained in the Arctic were lower ( $52\text{--}73\text{ nm}$  and  $10\text{ cm/s}$ , respectively), while the  $S_{\text{max}}$  values were generally higher ( $0.4\%$ ). In general, lower updraft velocities result in lower  $S_{\text{max}}$  and higher  $D_{\text{act}}$  values. However, in the Arctic, because of the very low aerosol concentrations,  $S_{\text{max}}$  values become higher and  $D_{\text{act}}$  values become lower, even under low  $W_{\text{eff}}$  conditions (the high- $S_{\text{max}}$  for low- $N_{\text{CCN}}$  mechanism, see equation (2)).

The high- $S_{\text{max}}$  for low- $N_{\text{CCN}}$  mechanism can also affect the ACI index. If  $S_{\text{max}}$  does not change with  $N_{70}$  (and everything else also does not change), then  $\text{dln}N_c/\text{dln}N_{70}$  achieves unity, and the ACI index has a maximum value of  $0.33$ . Figure 11 shows that the air parcel model calculation generally reproduces the observed relationship between  $N_{70}$  and  $N_c$  when a constant updraft velocity of  $10\text{ cm/s}$  is adopted. The model-calculated ACI index is  $0.26$ , which is similar to the observed ACI index values in the summer (June–August,  $T > 0^\circ\text{C}$ ) and winter–spring seasons (CCN-controlled data between December and April) of  $0.22 \pm 0.03$  and  $0.25 \pm 0.02$ , respectively (Table 2). When a higher or lower updraft velocity is assumed ( $50$  or  $2\text{ cm/s}$ ), the  $N_c$  values for the given  $N_{70}$  values increase or decrease (by a factor of  $2.4$  or  $0.54$ ), respectively; however, the slope (and therefore the ACI index) does not significantly change. The ACI index values are  $0.26$  and  $0.22$  for  $50$  and  $2\text{ cm/s}$  conditions, respectively. Furthermore, when pure sea-salt ( $\text{NaCl}$ ) or organic aerosols (oxalic acid as a surrogate compound), which are more or less hygroscopic than ammonium sulfate, respectively, are assumed for the aerosol composition, similar ACI index values of  $0.24$  or  $0.26$ , respectively, were obtained. The  $N_c/N_{70}$  ratios are higher or lower by approximately  $30\%$  when aerosol compositions that are more or less hygroscopic, respectively, are assumed. However, the sensitivity of cloud microphysics to aerosols, as evaluated by the ACI index, does not change significantly.



**Figure 14.** A time series of the monthly median values. (a)  $N_c$  and  $N_{70}$ , (b) CWC (cloud water content), and (c)  $r_e$  (cloud effective radius) for CCN-controlled data (both  $T > 0$  °C and  $T < 0$  °C) and CCN-uncontrolled data. Vertical bars indicate the 25th–75th percentiles. No data are available for April because simultaneous collection of clouds, aerosols, and meteorological data did not occur. CCN-uncontrolled data points are not shown for May–September because insufficient data were available (less than ten 1-hr data points). CCN = cloud condensation nuclei; DMPS = differential mobility particle sizer; SMPS = scanning mobility particle sizer.

The low sensitivity of the ACI index to the updraft velocity and aerosol composition may be in accordance with the simple approximation of the  $N_{CCN}$  dependence of  $N_c$  given in equation (3). When the updraft velocity and aerosol composition do not change with CCN concentration (these parameters are  $w$ ,  $k$ , and  $c$ , respectively, in equation (3)), the ACI index for adiabatic clouds can be approximated as follows:

$$ACI = \frac{1}{3} \frac{2}{k + 2} \quad (4)$$

Consequently, under these assumptions, ACI values do not depend on the updraft velocity and only weakly depend on aerosol composition. In fact, assuming typical  $k$  values between 0.4 and 1.0 (e.g., Rogers & Yau, 1989), derived ACI values between 0.22 and 0.28 are in agreement with the air parcel model calculations and observations (Table 2). We should note again that the ACI index values cannot be quantitatively explained

**Table 3**  
Results of the Air Parcel Model Calculations

$N_{70}$ range ( $\text{cm}^{-3}$ )	$N_{70}$ average ( $\text{cm}^{-3}$ )	Observation		Model calculation (variable $W$ )				Model calculation (constant $W$ )			
		$N_c$ average ( $\text{cm}^{-3}$ )	$D_{\text{act}}$ (nm)	$W_{\text{eff}}$ (cm/s)	$N_c$ ( $\text{cm}^{-3}$ )	$D_{\text{act}}$ (nm)	$S_{\text{max}}$ (%)	$W$ (cm/s)	$N_c$ ( $\text{cm}^{-3}$ )	$D_{\text{act}}$ (nm)	$S_{\text{max}}$ (%)
5–10	7.4	16.7	39.7	20	16.7	39.7	0.84	10	10.9	49.4	0.59
10–20	15.4	23.4	47.9	13	22.3	49.5	0.56	10	18.7	57.3	0.49
20–40	29.9	40.0	53.3	15	40.0	53.3	0.52	10	34.2	61.6	0.42
40–80	57.5	64.1	64.0	11	61.7	66.0	0.38	10	56.6	71.1	0.36
80–160	113.1	92.1	85.0	9	95.2	82.2	0.29	10	102.6	76.5	0.31
160–320	214.9	105.7	116.1	6	104.3	117.3	0.20	10	138.3	94.6	0.26

Note.  $N_{70}$  is the aerosol number concentration with dry diameters larger than 70 nm.  $N_c$  is the cloud particle number concentration.  $D_{\text{act}}$  is the threshold diameter of aerosol activation (the integrated aerosol number concentration greater than this diameter becomes equal to  $N_c$ ).  $W_{\text{eff}}$  is the vertical wind speed that results in the best agreement with the observed  $N_c$ .  $W$  is the assumed vertical wind speed for the calculations.  $S_{\text{max}}$  is the maximum supersaturation within an air parcel. For the input of the model calculations, the mountain base scanning mobility particle sizer aerosol data (June–August,  $T > 0$  °C) were used.

solely by the high- $S_{\text{max}}$  for low- $N_{\text{CCN}}$  mechanism; however, this simple mechanism could play an important role in controlling the relatively high sensitivities of the aerosol impacts on the low-level liquid clouds in the Arctic. We should also note that, although the ACI index does not significantly change, the  $N_c/N_{70}$  ratios do change by 30% when the aerosol composition changes within the ranges assumed in this study. Possible changes in aerosol chemical compositions are therefore an important factor for aerosol impacts on clouds.

## 5. Summary

Continuous in situ measurements of Arctic low-level clouds have been made at the Mount Zeppelin Observatory, which is located in Ny-Ålesund, Norway, since October 2013. Although the cloud particle measurements could be occasionally made under anisokinetic sampling conditions, the particle losses did not significantly affect the measurements, and therefore, we did not make any corrections to the data. Using this data set, we show the seasonal variations in the microphysical properties of clouds ( $N_c$ , CWC, and  $r_e$ ) and their relationships to the aerosol number concentrations ( $N_{70}$ ) by focusing on the ACI index values in summer (clean air) and winter–spring (Arctic haze).

In general, a good agreement between the aerosol measurements made at Mount Zeppelin (DMPS) and at the mountain base (SMPS at the Gruvebadet Observatory) was found when the number concentrations of the aerosols with dry diameters greater than 70 nm ( $N_{70}$ , a proxy for the CCN concentration) were compared. This agreement indicates that the aerosols within the cloud particles were successfully measured using the whole air inlet at Zeppelin. Although particle losses within the whole air inlet appeared to become significant when large-size cloud particles were present, the fraction of these data was small (10%), and therefore, we have not made any corrections to the DMPS data.

The monthly median  $N_c$  values showed a clear seasonal variation: Their maximum appeared in May–July ( $65 \pm 8 \text{ cm}^{-3}$ ) and then remained low between October and March ( $8 \pm 7 \text{ cm}^{-3}$ ). This seasonal variation in  $N_c$  generally follows that of  $N_{70}$ , although the  $N_c$  values were systematically lower than the  $N_{70}$  values between December and April.

At temperatures higher than 0 °C, the hourly  $N_c$  values were highly correlated with the  $N_{70}$  values. When clouds were detected below 0 °C, some of the data followed the summertime  $N_{70}$ - $N_c$  relationship, while others showed systematically lower  $N_c$  values. Lidar-derived depolarization ratios suggested that the former (CCN-controlled) and latter (CCN-uncontrolled) data generally corresponded to clouds consisting of supercooled water droplets and those containing ice particles ( $r < 23.5 \mu\text{m}$ ), respectively. The fraction of CCN-uncontrolled data (ice particles) was low (less than 20%) at temperatures higher than  $-4$  °C, while at temperatures between  $-4$  and  $-19$  °C, the CCN-uncontrolled data fraction was approximately 50%. When the temperature was lower than  $-19$  °C, this fraction reached 100%. Although the period when the atmospheric temperature was higher than 0 °C was short at Zeppelin, CCN-controlled data (water droplets) persistently appeared throughout the year.

The median threshold diameters of the aerosol activation ( $D_{\text{act}}$ ) for CCN-controlled clouds were 48 and 70 nm when DMPS (mountaintop) and SMPS (mountain base) aerosol data, respectively, were used. The threshold diameters were as low as 30–50 nm when  $N_{70}$  was  $<30 \text{ cm}^{-3}$ , indicating that small aerosols formed by new particle formation can affect the Arctic cloud microphysics.

The ACI index evaluated using  $N_c$  ( $\text{dln}N_c/(3\text{dln}N_{70})$ ) was  $0.22 \pm 0.03$  in summer (June–August,  $T > 0^\circ\text{C}$ ). A slightly higher ACI index of  $0.25 \pm 0.02$  was obtained in winter–spring (December–April); however, these values were within their mutual uncertainties. Previous studies showed that aerosols in summer and winter–spring are generally affected by new particle formation and anthropogenic emissions (Arctic haze), respectively. The results obtained in this study show that the ACI index values were not very different between these two periods (two aerosol sources). When the ACI index was calculated using  $r_e$  data ( $\text{dln}r_e/\text{dln}N_{70}$ ) for individual CWC ranges, a value of  $0.24 \pm 0.04$  was obtained (CCN-controlled data). These ACI estimates suggest that the previous estimates obtained from satellite measurements (0.0 to 0.19) underestimated the aerosol impacts on the cloud microphysics. The high ACI index values obtained in this study indicate that the CCN concentrations play an important role in controlling the microphysics of the liquid water clouds (and probably the mixed-phase clouds), which persistently appear at Mount Zeppelin throughout the year.

Using air parcel model calculations, we show that a simple cloud microphysical mechanism (high- $S_{\text{max}}$  for low- $N_{\text{CCN}}$  mechanism) can generally produce ACI index values similar to those determined from observations, although various parameters/processes can affect the aerosol-cloud interactions. This result is good news because this CCN activation process is readily implemented in numerical model calculations by adopting appropriate parameterizations, although a prediction of the probability density function of the updraft velocity is still a challenge. These numerical models can then be extended for mixed-phase clouds and/or used to study the consequences of the aerosol impacts on the Arctic clouds through various adjustments and feedback mechanisms.

### Appendix A: Wind Speed Around the Fog Monitor (FM-120)

The horizontal wind speed/direction statistics described in section 2.1 (Figure 3) were derived using 1-hr data obtained by the Vaisala anemometer (section 2.5 and Table 1). This instrument consists of a wind vane and a three-cup wheel and is located at an altitude of 15 m above the ground surface. Three-dimensional wind speed and direction were also measured at an altitude of 2.3 m above the ground surface using an ultrasonic anemometer (1 Hz, Table 1). Figure A1a shows the scatter plot between the horizontal wind speeds measured at altitudes of 15 and 2.3 m ( $U_{15}$  and  $U_{2.3}$ , respectively). Different symbol colors are used to show if data were obtained under southerly (wind direction between  $90^\circ$  and  $270^\circ$ ) or northerly (wind direction between  $-90^\circ$  and  $90^\circ$ ) wind conditions. The horizontal wind speeds near the ground surface (2.3 m) were systematically slower than those at the higher altitude (15 m): On average, the former were approximately one half to one third of the latter. The slower wind speeds near the ground were likely due to the friction of the ground surface. The even slower wind speeds under the northerly wind conditions than those under the southerly wind conditions were possibly because the ultrasonic anemometer was located near the southern edge of the mountain ridge and southerly winds were less affected by ground friction.

The fog monitor (FM-120) is located close to the ultrasonic anemometer (near the southern edge of the mountain ridge). The FM-120 inlet was oriented toward the south (prevailing wind direction), and its altitude was 1.4 m above the ground. As described in Appendix B, previous studies suggested that particle losses could take place in FM-120 measurements when both sampling angles and wind speeds are high. The results presented here (Figure A1a) indicate that wind speeds around the FM-120 ( $U_{2.3}$ ) were systematically slower than the meteorological wind data ( $U_{15}$ , Vaisala data), especially when sampling angles were large (northerly wind conditions). Consequently, particle losses could be smaller than those expected from meteorological data.

Figure A1b shows that there is a positive correlation between hourly horizontal wind speed at 15-m altitude and the root-mean-square of vertical wind speed variance ( $\overline{w'}$ ) measured at 2.3-m altitude. The vertical wind speed variance  $w'$  was defined as  $w' = w - \overline{w}$ , where  $w$  is 1-s vertical wind speed and  $\overline{w}$  is 61-s running mean. Hourly statistics of  $w'$  were used as a measure of eddy turbulence because histograms of 1-s  $w'$  values within

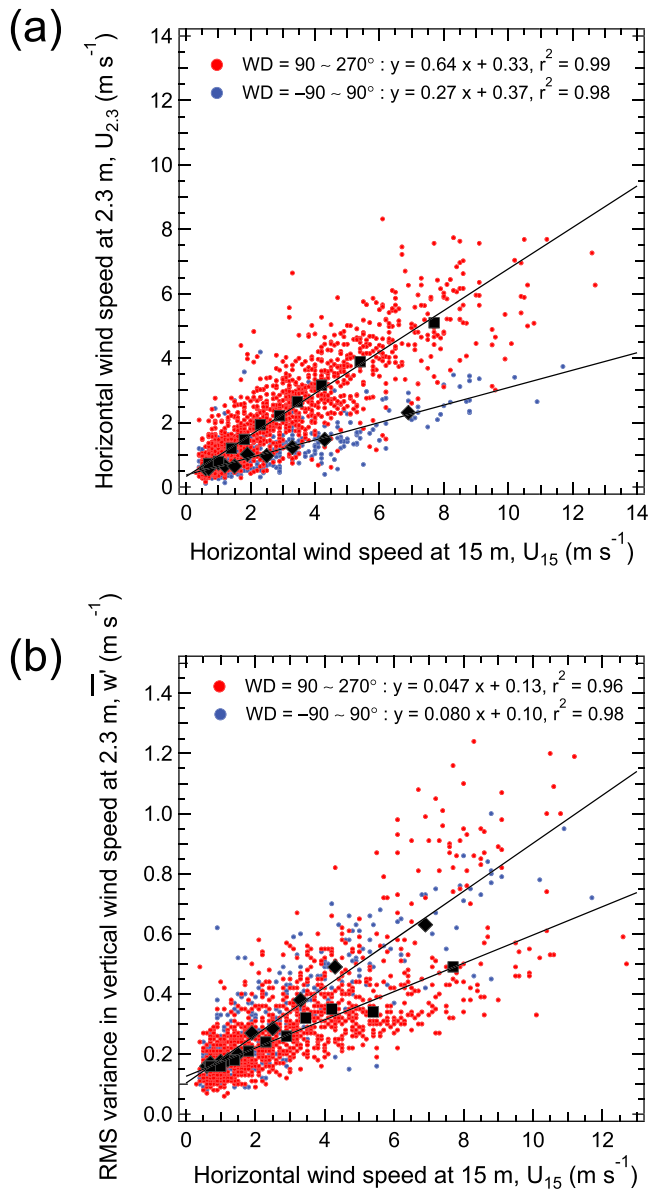


**Figure A1.** (a) A scatter plot between horizontal wind speed measurements made at altitudes of 15 and 2.3 m ( $U_{15}$  and  $U_{2.3}$  measured with the Vaisala and ultrasonic anemometers, respectively). Different symbol colors are used to show if data were obtained under southerly (wind direction, WD, between 90° and 270°) or northerly (WD between -90° and 90°) wind conditions. Black symbols indicate median values within individual data ranges, in which a similar number of data were obtained. Linear slopes and  $r^2$  values for these median values are given. (b) A scatter plot between horizontal wind speed measured at an altitude of 15 m ( $U_{15}$ ) and the root-mean-square (RMS) variance in vertical wind speed  $\overline{w'}$ . See the text for how this quantity was calculated.

individual 1-hr intervals generally show Gaussian distributions. Figure A1 b shows that  $\overline{w'}$  generally increases with increasing horizontal wind speed. This tendency was possibly due to the mechanical generation of turbulence from the horizontal wind, and topography could affect this generation. The slope was a factor of 1.7 greater under the northerly wind conditions, although the reasons are not clear. Notably, when horizontal wind speed measured at 2.3-m altitude is used to calculate the relationship with  $\overline{w'}$  instead of using 15-m data, the systematic differences in their slopes become even greater (the slope was a factor of 3.1 greater under the northerly wind conditions). The smaller differences in the slopes (more similar relationships between the horizontal wind speed and  $\overline{w'}$ ) between the northerly and southerly wind conditions may be more reasonable, suggesting that the level of the turbulence is not controlled by very local wind around the instruments but is more controlled by larger-scale meteorology. Because, in general, higher  $\overline{w'}$  can result in more numerous  $N_c$  from given aerosols, higher horizontal wind speed can result in an increase in  $N_c/N_{70}$ . However, a detailed study of  $\overline{w'}$  and its possible impact on cloud microphysics is beyond the scope of this study. In this study, this effect will be only examined when uncertainties in FM-120 measurements are examined (Appendix B).

### Appendix B: Uncertainties in the Fog Monitor (FM-120) Measurements

Incomplete sampling and/or losses of cloud particles can take place during FM-120 measurements (Spiegel et al., 2012). Previous studies suggested that particle losses decrease with increasing wind speed for sampling angles ( $\theta$ ) lower than 30°, while they increase with increasing wind speed for  $\theta > 30^\circ$  (Guyot et al., 2015). The previous study also suggested that for any wind speed greater than 3 m/s, the particle losses increase with particle diameter and sampling angle. In this study, possible errors in the  $N_c$  and CWC values obtained with FM-120 measurements caused by particle losses were evaluated in two ways as described below.

First, we compared the  $N_c$  and CWC values measured in  $2 \times 3 = 6$  conditions:  $\theta < \text{or} > 30^\circ$  and horizontal wind speeds ( $U_{2.3}$ ) of  $<2$ ,  $2\text{--}5$ , and  $>5$  m/s (Table B1). For the wind data, we used the ultrasonic anemometer data (from an altitude of 2.3 m) obtained near the FM-120 (whose inlet is at 1.4-m altitude) because meteorological data obtained at 15-m altitude (Figure 3, described in section 2.1) showed systematically higher horizontal wind speeds, as described in Appendix A. We used the data between June and August in 2015 with  $T > 0^\circ\text{C}$  because a number of cloud data available for statistical analyses was the highest and the ultrasonic anemometer data were also available in this time period. To eliminate the aerosol influences on the particle loss estimates, the  $N_{70}$  and  $N_c/N_{70}$  ratios are also shown for the DMPS and SMPS measurements (in the upper and lower parts, respectively, of the table).

When data with  $\theta > 30^\circ$  were examined, the  $N_c/N_{70}$  ratios increased with increasing horizontal wind speed (Table B1). This tendency contradicts the theoretical expectation of particle losses; therefore, the influences of particle losses on  $N_c$  are considered to be small. We speculate that this increasing tendency in the  $N_c/N_{70}$  ratios was because higher horizontal wind speeds resulted in higher updraft velocities within turbulent air (Appendix A), which generally result in more numerous  $N_c$  from given aerosols (higher  $N_c/N_{70}$  ratios).

**Table B1**

Median Values of  $N_c$  and CWC for the Six Wind Speed/Direction Categories (June–August 2015,  $T > 0^\circ\text{C}$ )

Sampling angle $\theta$	Horizontal wind speed at 2.3 m, $U_{2.3}$ (m/s)	Number of data	$N_c$ ( $\text{cm}^{-3}$ )	CWC ( $\text{gm}^{-3}$ )	$N_{70}$ ( $\text{cm}^{-3}$ )	$N_c/N_{70}$	$N_{c,r} > 12.5\mu\text{m}/N_c$	$\text{CWC}_{r > 12.5\mu\text{m}}/\text{CWC}$
Aerosol: DMPS (mountaintop)								
$\theta < 30^\circ$	$U_{2.3} < 2$	105	50.0	0.074	60.3	1.22	5.56e-03	4.91e-02
	$U_{2.3} = 2-5$	70	52.9	0.072	30.1	1.94	4.21e-03	2.80e-02
	$U_{2.3} > 5$	32	102.6	0.042	53.8	2.04	1.45e-04	4.91e-03
$\theta > 30^\circ$	$U_{2.3} < 2$	174	56.6	0.072	79.4	0.83	8.18e-04	6.67e-03
	$U_{2.3} = 2-5$	7	32.5	0.041	15.1	2.30	1.63e-04	2.24e-03
	$U_{2.3} > 5$	0						
Aerosol: SMPS (mountain base)								
$\theta < 30^\circ$	$U_{2.3} < 2$	133	48.1	0.065	65.7	0.80	2.97e-03	2.42e-02
	$U_{2.3} = 2-5$	102	48.2	0.070	37.6	1.32	4.09e-03	3.08e-02
	$U_{2.3} > 5$	36	102.4	0.036	56.2	1.66	1.35e-04	4.36e-03
$\theta > 30^\circ$	$U_{2.3} < 2$	203	53.0	0.072	69.9	0.79	1.01e-03	8.92e-03
	$U_{2.3} = 2-5$	14	27.4	0.069	27.9	1.30	1.21e-02	3.45e-02
	$U_{2.3} > 5$	0						

Note. For wind data, those measured with the ultrasonic anemometer (2.3-m altitude) near the fog monitor (FM-120) are used. The Vaisala meteorological wind speed data (Figure 3) were not used because their values measured at an altitude of 15 m were systematically higher (Appendix A). Sampling angle ( $\theta$ ) is the angle between the inlet orientation (south) and the wind vector.  $N_{70}$  is the integrated number concentration of aerosols with dry diameters greater than 70 nm. Analyses were made using 1-hr data. CWC = cloud water content; DMPS = differential mobility particle sizer; SMPS = scanning mobility particle sizer.

Notably, a fraction of the data with  $U_{2.3} > 2$  m/s is low within the  $\theta > 30^\circ$  data set (5%) during the time period we examined here, partly due to the higher reduction rate of the horizontal wind speed near the ground surface under the northerly wind conditions (Appendix A). Consequently, data sampled under unfavorable air sampling conditions ( $\theta > 30^\circ$  and  $U_{2.3} > 2$  m/s) had little effect on our statistical analyses, even when particle losses occurred.

When data with  $\theta < 30^\circ$  were examined,  $N_c/N_{70}$  ratios for  $U_{2.3} = 2-5$  and  $< 2$  m/s were lower by 5–20 and 40–48%, respectively, than those for  $U_{2.3} > 5$  m/s. These results are generally in accordance with the results of the previous study (Guyot et al., 2015), for example, higher particle loss rates (lower  $N_c/N_{70}$  ratios) appeared for lower wind speeds for  $\theta < 30^\circ$ . However, as shown above (analysis of the  $\theta > 30^\circ$  data set), higher horizontal wind speed can result in higher  $N_c/N_{70}$  ratios through higher updraft velocity. Furthermore, when the shape of the particle size distribution was examined, the relative fractions of cloud particles with large radii ( $r > 12.5 \mu\text{m}$ ,  $N_{c,r} > 12.5\mu\text{m}/N_c$ ) were generally higher for lower horizontal wind speeds (Table B1), although loss rates are expected to be higher for the larger particles. These results suggest that the observed lower  $N_c$  values (lower  $N_c/N_{70}$  ratios) for lower horizontal wind speeds may not be solely due to particle losses and may be partly due to other factors, such as lower updraft velocities. Consequently, quantitative estimates of the effect of particle losses on the  $N_c$  measurements for the  $\theta < 30^\circ$  condition cannot be made in this study.

We also examined the wind speed dependence of the CWC values for both the  $\theta < 30^\circ$  and  $\theta > 30^\circ$  conditions (Table B1). Although the CWC values may not directly depend on  $N_{70}$  values, statistical analyses were performed on simultaneous measurements of the FM-120 and DMPS or SMPS, similar to the  $N_c$  analyses. For  $\theta < 30^\circ$ , the CWC values generally decreased with increasing horizontal wind speed, thus suggesting no particle loss influences. For  $\theta > 30^\circ$ , the CWC values decreased with increasing horizontal wind speed when DMPS data were used. When the shapes of the particle size distributions were examined, the relative contributions of the CWC from the cloud particles with large radii ( $\text{CWC}_{r > 12.5\mu\text{m}}/\text{CWC}$ ) were generally lower for the higher horizontal wind speed (DMPS data in Table B1). These tendencies are in accordance with the previous study, namely, higher loss rates of larger particles. However, these tendencies were not clearly observed when SMPS data were used. Furthermore, CWC values for  $\theta > 30^\circ$  were not necessarily lower than those for  $\theta < 30^\circ$ , which are considered to be more reliable. Consequently, quantitative estimates of the particle losses cannot be made in this study. We also note that, in general, the CWC value increases with increasing altitude above the cloud base, and this effect needs to be eliminated for the quantitative evaluation of the particle losses. The cloud base height was

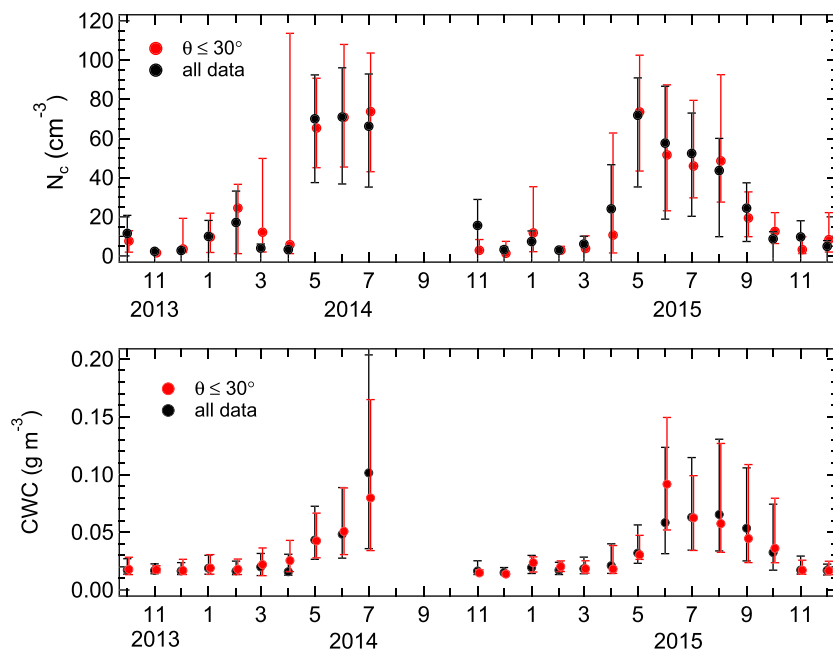


**Figure B1.** A time series of the monthly median values of (a)  $N_c$  and (b) CWC (cloud water content). The black and red circles denote values derived using all of the data irrespective of the wind direction and those obtained only using data with sampling angles  $<30^\circ$ , respectively. The former values were used in this study (the  $N_c$  values shown in black are the same as those shown in Figure 6a). The latter values were obtained under more reliable measurement conditions; however, the number of measurements was limited. Vertical bars indicate the 25th–75th percentiles.

examined for the six wind speed/direction-categorized data sets using the ceilometer measurements; however, very large variations were found. Based on these results, we have not made any corrections to the data and have not rejected any data in this study. In fact, any corrections of the particle losses that depend on the wind direction/speed and phase of the cloud particles can lead to further uncertainties.

As the second way to evaluate uncertainties due to particle losses, we compared the monthly median  $N_c$  and CWC values shown in this study (derived using all of the data irrespective of the wind speed or direction) with those obtained using only the data with sampling angles  $<30^\circ$  ( $N_{c_{\theta < 30}}$  and  $CWC_{\theta < 30}$ ) because the latter is considered to be more reliable (Figure B1). Note that for the analyses described above in this appendix, we used only data obtained between June and August with  $T > 0^\circ\text{C}$ , while we used all of the data for the analyses described here. As shown in Figure B1, the monthly median values of  $N_{c_{\theta < 30}}$  ( $CWC_{\theta < 30}$ ) were sometimes above and sometimes below the  $N_c$  (CWC) values derived from all of the data. The median values of the  $N_c/N_{c_{\theta < 30}}$  and  $CWC/CWC_{\theta < 30}$  ratios were 1.05 (with a 25–75% range of 0.77–1.50) and 1.00 (with a 25–75% range of 0.91–1.06), respectively, suggesting that, on average, the errors due to the particle losses were less than 5%. The influences from the particle losses in the FM-120 measurements depend on the size distribution (and possibly the phase) of the cloud particles. At Zeppelin, the number fractions of the cloud particles with large radii ( $r > 12.5\ \mu\text{m}$ ) within all of the cloud particles ( $N_{c,r > 12.5}/N_c$ ) were less than 1% and 10% for 49.2% and 63.4%, respectively, of the cloud data. This result indicates that the number fractions of the large cloud particles are generally not very large, which could result in a relatively small error in the FM-120 measurements.

### Appendix C: Uncertainties in Using the Whole Air Inlet

The whole air inlet was used for the aerosol size distribution measurements with the DMPS at the Mount Zeppelin Observatory (section 2.4). Aerosols within the cloud particles are assumed to be measured (together with the interstitial aerosols) by evaporating the water of these particles within the heated inlet tube. However, when the  $N_{70}$  values were compared between the DMPS (mountaintop) and the SMPS

**Table C1**

Median Values of the  $N_{70\_DMPS}/N_{70\_SMPS}$  Ratios for three Wind Speed and Two Cloud Particle Size Distribution ( $N_{c,r} > 12.5\mu\text{m}/N_c$ ) Categories

Horizontal wind speed at 15 m, $U_{15}$ ( $\text{m s}^{-1}$ )	$N_{c,r} >$ $12.5\mu\text{m}/N_c$	$T > 0^\circ\text{C}$ (June–August)		$T < -4^\circ\text{C}$ (all months)	
		Number of data	$N_{70\_DMPS}/N_{70\_SMPS}$	Number of data	$N_{70\_DMPS}/N_{70\_SMPS}$
$U_{15} < 2$	<0.2	214	1.01	60	0.72
	>0.2	29	0.39	0	—
	all	243	0.97	60	0.72
$U_{15} = 2\text{--}5$	<0.2	140	0.83	32	0.94
	>0.2	14	0.15	9	0.99
	all	154	0.80	41	0.96
$U_{15} > 5$	<0.2	60	0.92	42	0.78
	>0.2	3	0.15	37	0.85
	all	63	0.91	79	0.84
All data	<0.2	414	0.94	134	0.81
	>0.2	46	0.29	46	0.86
	all	460	0.91	180	0.84

*Note.* For wind data, the Vaisala meteorological data at 15-m altitude are used because the whole air inlet is approximately 2.5 m above the roof of the observatory building and a time coverage of this data set is longer than that of the ultrasonic anemometer data.  $N_{70}$  is the integrated number concentration of aerosols with dry diameters greater than 70 nm.  $N_{70\_DMPS}$  and  $N_{70\_SMPS}$  are the  $N_{70}$  values obtained by DMPS (mountaintop) and SMPS (mountain base), respectively. Analyses were made using 1-hr data. DMPS = differential mobility particle sizer; SMPS = scanning mobility particle sizer.

(mountain base) measurements, systematically lower DMPS values were occasionally observed when the data were obtained under cloudy conditions (Figure 4b, section 2.4). These lower DMPS values could be real if air sampled at the top and base of the mountain had different air mass histories when clouds appeared at Mount Zeppelin and/or precipitation removed aerosols within the upper layer. However, systematic differences suggest that there was incomplete sampling and/or losses of the cloud particles within the whole air inlet, especially when particles with large radii were present and/or the wind speed was high. Table C1 shows the median values of  $N_{70\_DMPS}/N_{70\_SMPS}$  ratios for the  $3 \times 2 = 6$  categories for the in-cloud data set: Wind speeds ( $U_{15}$ ) of <2, 2–5, and >5 m/s and the relative fractions of the cloud particles with large radii ( $r > 12.5 \mu\text{m}$ ,  $N_{c,r} > 12.5\mu\text{m}/N_c$ ) of <0.2 and >0.2. The values are shown for both  $T > 0^\circ\text{C}$  (June–August only) and  $T < -4^\circ\text{C}$  conditions (with no restriction on the month of the year). Clouds in the former conditions likely consisted of liquid droplets, while those in the latter conditions could contain ice particles (section 3.5). For wind data, the Vaisala meteorological data at 15-m altitude are used.

The  $T > 0^\circ\text{C}$  data were examined first. For 90% of the data, the  $N_{c,r} > 12.5\mu\text{m}/N_c$  ratios were less than 0.2, and in these cases, the  $N_{70\_DMPS}/N_{70\_SMPS}$  ratios were 0.83 to 1.01 (Table C1). This result suggests that in most cases, the particle losses were less than 20% due to the dominance of small cloud particles even when the wind speeds were high ( $U_{15} > 5$  m/s). However, for 10% of the data,  $N_{c,r} > 12.5\mu\text{m}/N_c$  ratios were higher than 0.2, and the loss of particles could be up to 61% and 85% for  $U < 2$  and  $>5$  m/s, respectively. These data resulted in systematically lower DMPS-derived  $N_{70}$  values compared with the SMPS values shown in Figure 4b. However, because the fraction of the data with high  $N_{c,r} > 12.5\mu\text{m}/N_c$  ratios was small (10%), we have not made any corrections to the data and have not rejected any data in this study.

On the other hand, for the  $T < -4^\circ\text{C}$  conditions, no clear dependences of the  $N_{70\_DMPS}/N_{70\_SMPS}$  ratios on either the wind speed or the  $N_{c,r} > 12.5\mu\text{m}/N_c$  ratios were found, although the number of data was limited (Table C1). When all  $T < -4^\circ\text{C}$  data were examined, irrespective of the wind speed, the median  $N_{70\_DMPS}/N_{70\_SMPS}$  ratios were found to be 0.81 and 0.86 for the data sets with  $N_{c,r} > 12.5\mu\text{m}/N_c$  ratios of <0.2 and >0.2, respectively. These results suggest that the particle loss rates were generally lower for the ice particles, which tend to move with the air.

Finally, similar analyses were made using the no-cloud data. The median  $N_{70\_DMPS}/N_{70\_SMPS}$  ratios did not change with the wind speed and were 0.96–0.97 for the three wind conditions, that is, <2, 2–5, and >5 m/s, suggesting that the wind did not affect the aerosol sampling when there were no clouds (not shown).

## Acknowledgments

We thank Ikuyo Oshima for her contributions to the data analysis. This study was supported by the Ministry of Education, Culture, Sports, Science, and Technology (MEXT) in Japan (the GRENE Arctic Climate Change Research Project and ArCS Project) and the Japan Society for the Promotion of Science (JSPS) KAKENHI Grants (JP26241003). This research was also supported by the Environment Research and Technology Development Fund (2-1703) of the Environmental Restoration and Conservation Agency. We also thank the staff of the Norwegian Polar Institute for the maintenance of the cloud and aerosol measurements at Mount Zeppelin. Stockholm University also acknowledges the Swedish EPA for supporting the work at the Zeppelin station. We thank the reviewers for providing useful comments and suggestions. Cloud particle and aerosol concentration data are available through the ArCS/ADS (Arctic Data archive System, <https://ads.nipr.ac.jp/portal/index.action>): FM-120 data (<https://ads.nipr.ac.jp/dataset/A20181011-002>), DMPS data (<https://ads.nipr.ac.jp/dataset/A20181011-001>), and SMPS data (<https://ads.nipr.ac.jp/dataset/A20181011-003>). Ceilometer and meteorological data are available from the following URLs: <https://www.earth-syst-sci-data.net/10/1451/2018/essd-10-1451-2018.html> and <http://ebas.nilu.no/Default.aspx>, respectively.

## References

- Beine, H. J., Argentini, S., Maurizi, A., Mastrantonio, G., & Viola, A. (2001). The local wind field at Ny-Alesund and the Zeppelin mountain at Svalbard. *Meteorology and Atmospheric Physics*, 78(1–2), 107–113. <https://doi.org/10.1007/s007030170009>
- Bringi, V., Thurai, M., & Baumgardner, D. (2018). Raindrop fall velocities from an optical array probe and 2-D video disdrometer. *Atmospheric Measurement Techniques*, 11, 1377–1384. <https://doi.org/10.5194/amt-11-1377-2018>
- Brock, C. A., Cozic, J., Bahreini, R., Froyd, K. D., Middlebrook, A. M., McComiskey, A., et al. (2011). Characteristics, sources, and transport of aerosols measured in spring 2008 during the aerosol, radiation, and cloud processes affecting Arctic Climate (ARCPAC) Project (2011). *Atmospheric Chemistry and Physics*, 11, 2423–2453. <https://doi.org/10.5194/acp-11-2423-2011>
- Coopman, Q., Garrett, T. J., Finch, D. P., & Riedi, J. (2018). High sensitivity of arctic liquid clouds to long-range anthropogenic aerosol transport. *Geophysical Research Letters*, 45(1), 372–381. <https://doi.org/10.1002/2017GL075795>
- Coopman, Q., Garrett, T. J., Riedi, J., Eckhardt, S., & Stohl, A. (2016). Effects of long-range aerosol transport on the microphysical properties of low-level liquid clouds in the Arctic. *Atmospheric Chemistry and Physics*, 16, 4661–4674. <https://doi.org/10.5194/acp-16-4661-2016>
- Curry, J. A., & Ebert, E. E. (1992). Annual cycle of radiation fluxes over the Arctic Ocean: Sensitivity to cloud optical properties. *Journal of Climate*, 5(11), 1267–1280. [https://doi.org/10.1175/1520-0442\(1992\)005<1267:ACORFO>2.0.CO;2](https://doi.org/10.1175/1520-0442(1992)005<1267:ACORFO>2.0.CO;2)
- de Boer, G., Eloranta, E. W., & Shupe, M. D. (2009). Arctic mixed-phase stratiform cloud properties from multiple years of surface-based measurements at two high-latitude locations. *Journal of the Atmospheric Sciences*, 66, 2874–2887. <https://doi.org/10.1175/2009JAS3029.1>
- Di Liberto, L., Angelini, F., Pietroni, I., Cairo, F., Di Donfrancesco, G., Viola, A., et al. (2012). Estimate of the Arctic convective boundary layer height from lidar observations: A case study. *Advances in Meteorology*, 2012, 851927. <https://doi.org/10.1155/2012/851927>
- Engvall, A.-C., Krejci, R., Ström, J., Treffeisen, R., Scheele, R., Hermansen, O., & Paatero, J. (2008). Changes in aerosol properties during spring-summer period in the Arctic troposphere. *Atmospheric Chemistry and Physics*, 8, 445–462. <https://doi.org/10.5194/acp-8-445-2008>
- Esau, I., & Repina, I. (2012). Wind climate in Kongsfjorden, Svalbard, and attribution of leading wind driving mechanisms through turbulence-resolving simulations. *Advances in Meteorology*, 2012, 568454. <https://doi.org/10.1155/2012/568454>
- Fan, J., Rosenfeld, D., Zhang, Y., Giangrande, S. E., Li, Z., Machado, L. A. T., et al. (2018). Substantial convection and precipitation enhancements by ultrafine aerosol particles. *Science*, 359, 411–418. <https://doi.org/10.1126/science.aan8461>
- Feingold, G., & Heymsfield, A. J. (1992). Parameterizations of condensational growth of droplets for use in general circulation models. *Journal of the Atmospheric Sciences*, 49, 2325–2342.
- Garrett, T. J., & Zhao, C. (2006). Increased Arctic cloud longwave emissivity associated with pollution from mid-latitudes. *Nature*, 440, 787–789. <https://doi.org/10.1038/nature04636>
- Garrett, T. J., Zhao, C., Dong, X., Mace, G. G., & Hobbs, P. V. (2004). Effects of varying aerosol regimes on low-level Arctic stratus. *Geophysical Research Letters*, 31, L17105. <https://doi.org/10.1029/2004GL019928>
- Gayet, J.-F., Treffeisen, R., Helbig, A., Bareiss, J., Matsuki, A., Herber, A., & Schwarzenboeck, A. (2009). On the onset of the ice phase in boundary layer Arctic clouds. *Journal of Geophysical Research*, 114(D19), D19201. <https://doi.org/10.1029/2008JD011348>
- Graversen, R. G., & Wang, M. (2009). Polar amplification in a coupled climate model with locked albedo. *Climate Dynamics*, 33(5), 629–643. <https://doi.org/10.1007/s00382-009-0535-6>
- Gulstepe, I., Kuhn, T., Pavolonis, M., Calvert, C., Gurka, J., Heymsfield, A. J., et al. (2014). Ice fog in Arctic during Fram-Ice Fog project. *Bulletin of the American Meteorological Society*, 91, 211–226. <https://doi.org/10.1175/BAMS-D-11-00071.1>
- Guyot, G., Gourbeyre, C., Febvre, G., Shcherbakov, V., Burnet, F., Dupont, J.-C., et al. (2015). Quantitative evaluation of seven optical sensors for cloud microphysical measurements at the Puy-de-Dôme Observatory, France. *Atmospheric Measurement Techniques*, 8, 4347–4367. <https://doi.org/10.5194/amt-8-4347-2015>
- Hudson, J. G., Noble, S., & Jha, V. (2010). Stratus cloud supersaturations. *Geophysical Research Letters*, 37, L21813. <https://doi.org/10.1029/2010GL045197>
- Intrieri, J. M., Shupe, M. D., Uttal, T., & McCarty, B. J. (2002). An annual cycle of Arctic cloud characteristics observed by radar and lidar at SHEBA. *Journal of Geophysical Research*, 107(C10), 8030. <https://doi.org/10.1029/2000JD000423>
- IPCC (2013). *Climate change 2013: The physical science basis. Contribution of Working Group I to the Fourth Assessment Report of the Intergovernmental Panel on Climate Change*. Cambridge, UK: Cambridge University Press.
- Jackson, R. C., McFarquhar, G. M., Korolev, A. V., Earle, M. E., Liu, P. S. K., Lawson, R. P., et al. (2012). The dependence of ice microphysics on aerosol concentration in arctic mixed-phase stratus clouds during ISDAC and M-PACE. *Journal of Geophysical Research*, 117, D15207. <https://doi.org/10.1029/2012JD017668>
- Jourdan, O., Mioche, G., Garrett, T. J., Schwarzenböck, A., Vidot, J., Xie, Y., et al. (2010). Coupling of the microphysical and optical properties of an Arctic nimbostratus cloud during the ASTAR 2004 experiment: Implications for light-scattering modeling. *Journal of Geophysical Research*, 115, D23206. <https://doi.org/10.1029/2010JD014016>
- Klingebiel, M., de Lozar, A., Molleker, S., Weigel, R., Roth, A., Schmidt, L., et al. (2015). Arctic low-level boundary layer clouds: In situ measurements and simulations of mono- and bimodal supercooled droplet size distributions at the top layer of liquid phase clouds. *Atmospheric Chemistry and Physics*, 15(2), 617–631. <https://doi.org/10.5194/acp-15-617-2015>
- Knollenberg, R. (1970). The optical array: An alternative to scattering or extinction for airborne particle size determination. *Journal of Applied Meteorology*, 9(1), 86–103. [https://doi.org/10.1175/1520-0450\(1970\)009<0086:TOAAAT.2.0.CO;2](https://doi.org/10.1175/1520-0450(1970)009<0086:TOAAAT.2.0.CO;2)
- Knollenberg, R. (1981). Techniques for probing cloud microstructure. In P. V. Hobbs & A. Deepak (Eds.), *Clouds, their formation, optical properties and effects* (pp. 15–91). Oxford, UK: Academic Press.
- Koike, M., Takegawa, N., Moteki, N., Kondo, Y., Nakamura, H., Kita, K., et al. (2012). Measurements of regional-scale aerosol impacts on cloud microphysics over the East China Sea: Possible influences of warm sea surface temperature over the Kuroshio Ocean current. *Journal of Geophysical Research*, 117, D17205. <https://doi.org/10.1029/2011JD017324>
- Leaitch, W. R., Korolev, A., Aliabadi, A. A., Burkart, J., Willis, M. D., Abbatt, J. P. D., et al. (2016). Effects of 20–100 nm particles on liquid clouds in the clean summertime Arctic. *Atmospheric Chemistry and Physics*, 16, 11,107–11,124. <https://doi.org/10.5194/acp-16-11107-2016>
- Lihavainen, H., Kerminen, V.-M., & Remer, L. A. (2010). Aerosol-cloud interaction determined by both in situ and satellite data over a northern high-latitude site. *Atmospheric Chemistry and Physics*, 10, 987–10,995. <https://doi.org/10.5194/acp-10-10987-2010>
- Lohmann, U., & Feichter, J. (2005). Global indirect aerosol effects: A review. *Atmospheric Chemistry and Physics*, 5(3), 715–737. <https://doi.org/10.5194/acp-5-715-2005>

- Lubin, D., & Vogelmann, A. M. (2006). A climatologically significant aerosol longwave indirect effect in the Arctic. *Nature*, *439*(7075), 453–456. <https://doi.org/10.1038/nature04449>
- Lupi, A., Busetto, M., Becagli, S., Giardi, F., Lanconelli, C., Mazzola, M., et al. (2016). Multi-seasonal ultrafine aerosol particle number concentration measurements at the Gruvebadet observatory, Ny-Ålesund, Svalbard Islands. *Rendiconti Fisiche Accademia dei Lincei*, *27*, 59–S71. <https://doi.org/10.1007/s12210-016-0532-8>
- Maturilli, M., & Ebell, K. (2018). Twenty-five years of cloud base height measurements by ceilometer in Ny-Ålesund, Svalbard. *Earth System Science Data*, *10*, 1451–1456. <https://doi.org/10.5194/essd-10-1451-2018>
- Mauritsen, T., Sedlar, J., Tjernström, M., Leck, C., Martin, M., Shupe, M., et al. (2011). An Arctic CCN-limited cloud-aerosol regime. *Atmospheric Chemistry and Physics*, *11*, 165–173. <https://doi.org/10.5194/acp-11-165-2011>
- McComiskey, A., & Feingold, G. (2012). The scale problem in quantifying aerosol indirect effects. *Atmospheric Chemistry and Physics*, *12*, 1031–1049. <https://doi.org/10.5194/acp-12-1031-2012>
- McFarquhar, G. M., Ghan, S., Verlinde, J., Korolev, A., Strapp, J. W., Schmid, B., et al. (2011). Indirect and semi-direct aerosol campaign. *Bulletin of the American Meteorological Society*, *88*, 205–221.
- Palm, S. P., Strey, S. T., Spinhirne, J., & Markus, T. (2010). Influence of Arctic Sea ice extent on polar cloud fraction and vertical structure and implications for regional climate. *Journal of Geophysical Research*, *115*, D21209. <https://doi.org/10.1029/2010JD013900>
- Quaas, J., Ming, Y., Menon, S., Takemura, T., Wang, M., Penner, J. E., et al. (2009). Aerosol indirect effects—General circulation model intercomparison and evaluation with satellite data. *Atmospheric Chemistry and Physics*, *9*, 8697–8717. <https://doi.org/10.5194/acp-9-8697-2009>
- Quinn, P. K., Collins, D. B., Grassian, V. H., Prather, K. A., & Bates, T. S. (2015). Chemistry and related properties of freshly emitted sea spray aerosol. *Chemical Reviews*, *115*, 4383–4399. <https://doi.org/10.1021/cr500713g>
- Rogers, R. R., & Yau, M. K. (1989). *A short course in cloud physics*, (3rd ed.). Oxford, UK: Elsevier Science. ISBN: 0-7506-3215-1.
- Serreze, M. C., & Barry, R. G. (2011). Processes and impacts of Arctic amplification: A research synthesis. *Global and Planetary Change*, *77*(1-2), 85–96. <https://doi.org/10.1016/j.gloplacha.2011.03.004>
- Shiobara, M., Yabuki, M., & Kobayashi, H. (2003). A polar cloud analysis based on micro-pulse lidar measurements at Ny-Alesund, Svalbard and Syowa, Antarctica. *Physics and Chemistry of the Earth*, *28*(28-32), 1205–1212. <https://doi.org/10.1016/j.pce.2003.08.057>
- Shupe, M. D. (2007). A ground-based multisensor cloud phase classifier. *Geophysical Research Letters*, *34*, L22809. <https://doi.org/10.1029/2007GL031008>
- Shupe, M. D. (2011). Clouds at Arctic atmospheric observatories. Part II: Thermodynamic phase characteristics. *Journal of Applied Meteorology and Climatology*, *50*, 645–661. <https://doi.org/10.1175/2010JAMC2468.1>
- Spiegel, J. K., Zieger, P., Bukowiecki, N., Hammer, E., Weingartner, E., & Eugster, W. (2012). Evaluation the capabilities and uncertainties of droplet measurements for the fog droplet spectrometer (FM-100). *Atmospheric Measurement Techniques*, *5*, 2237–2260. <https://doi.org/10.5194/amt-5-2237-2012>
- Strom, J., Umegard, J., Torseth, K., Tunved, P., Hansson, H. C., Holmen, K., et al. (2003). One year of particle size distribution and aerosol chemical composition measurements at the Zeppelin Station, Svalbard, March 2000–March 2001. *Physics and Chemistry of the Earth*, *28*(28-32), 1181–1190. <https://doi.org/10.1016/j.pce.2003.08.058>
- Sugimoto, N., Matsui, I., Liu, Z., Shimizu, A., Yoneyama, K., & Katsumata, M. (2001). Latitudinal distribution of aerosols and clouds in the western Pacific observed with a lidar on board the. *Geophysical Research Letters*, *28*(22), 4187–4190. <https://doi.org/10.1029/2001GL013510>
- Tietze, K., Riedi, J., Stohl, A., & Garrett, T. J. (2011). Space-based evaluation of interactions between aerosols and low-level Arctic clouds during the spring and summer of 2008. *Atmospheric Chemistry and Physics*, *11*, 3359–3373. <https://doi.org/10.5194/acp-11-3359-2011>
- Tunved, P., Strom, J., & Krejci, R. (2013). Arctic aerosol life cycle: Linking aerosol size distributions observed between 2000 and 2010 with air mass transport and precipitation at Zeppelin station, Ny-Alesund, Svalbard. *Atmospheric Chemistry and Physics*, *13*, 3643–3660. <https://doi.org/10.5194/acp-13-3643-2013>
- Twomey, S. (1959). The nuclei of natural cloud formation. Part II: The supersaturation in natural clouds and the variation of cloud droplet concentration. *Pure and Applied Geophysics*, *43*, 243–249.
- Twomey, S. (1977). The influence of pollution on the shortwave albedo of clouds. *Journal of the Atmospheric Sciences*, *34*(7), 1149–1152. [https://doi.org/10.1175/1520-0469\(1977\)034<1149:TIOPOT>2.0.CO;2](https://doi.org/10.1175/1520-0469(1977)034<1149:TIOPOT>2.0.CO;2)
- Uchiyama, A., Yamazaki, A., Shiobara, M., & Kobayashi, H. (2014). Case study on microphysical properties of boundary layer mixed-phase cloud observed at Ny-Ålesund, Svalbard: Observed cloud microphysics and calculated optical properties on 9 June 2011. *Polar Science*, *8*, 57–72. <https://doi.org/10.1016/j.polar.2013.11.001>
- Verlinde, J., Harrington, J. Y., McFarquhar, G. M., Yannuzzi, V. T., Avramov, A., Greenberg, S., et al. (2007). The mixed-phase Arctic cloud experiment. *Bulletin of the American Meteorological Society*, *92*, 183–201. <https://doi.org/10.1175/BAMS-88-2-205>
- Weinbruch, S., Wiesemann, D., Ebert, M., Schütze, K., Kallenborn, R., & Ström, J. (2012). Chemical composition and sources of aerosol particles at Zeppelin Mountain (Ny Ålesund, Svalbard): An electron microscopy study. *Atmospheric Environment*, *49*, 142–150. <https://doi.org/10.1016/j.atmosenv.2011.12.008>
- Weingartner, E., Nyeki, S., & Baltensperger, U. (1999). Seasonal and diurnal variation of aerosol size distributions ( $10 < D < 750$  nm) at a high-alpine site (Jungfrauch 3580 m asl). *Journal of Geophysical Research*, *104*(D21), 26,809–26,820. <https://doi.org/10.1029/1999JD900170>
- Young, G., Jones, H. M., Choulaton, T. W., Crosier, J., Bower, K. N., Gallagher, M. W., et al. (2016). Observed microphysical changes in Arctic mixed-phase clouds when transitioning from sea ice to open ocean. *Atmospheric Chemistry and Physics*, *16*, 13,945–13,967. <https://doi.org/10.5194/acp-16-13945-2016>
- Zamora, L. M., Kahn, R. A., Cubison, M. J., Diskin, G. S., Jimenez, J. L., Kondo, Y., et al. (2016). Aircraft-measured indirect cloud effects from biomass burning smoke in the Arctic and subarctic. *Atmospheric Chemistry and Physics*, *16*, 715–738. <https://doi.org/10.5194/acp-16-715-2016>